INTERNATIONAL JOURNAL OF
NUMERICAL ANALYSIS AND MODELING
Volume 6, Number 4, Pages 533–561

DISCONTINUOUS GALERKIN METHODS FOR CONVECTION-DIFFUSION EQUATIONS FOR VARYING AND VANISHING DIFFUSIVITY

J. PROFT AND B. RIVIÈRE

Abstract. This work formulates and analyzes a new family of discontinuous Galerkin methods for the time-dependent convection-diffusion equation with highly varying diffusion coefficients, that do not require the use of slope limiting techniques. The proposed methods are based on the standard NIPG/SIPG techniques, but use special diffusive numerical fluxes at some important interfaces. The resulting numerical solutions have an L^2 error that is significantly smaller than the error obtained with standard discontinuous Galerkin methods. Theoretical convergence results are also obtained.

Key Words. numerical fluxes, discontinuous Galerkin methods, high and low diffusivity, L^2 error

1. Introduction and Problem Definition

In this work we explore the development and analysis of discontinuous Galerkin methods applied to the solution of linear advection-diffusion equations

$$\partial_t u + \nabla \cdot (\beta u - \epsilon \nabla u) = f, \qquad \text{in} \quad \Omega \times (0, T). \tag{1}$$

Although problems of this type occur in many applications, we are primarily motivated by the modeling of flow in porous media such as petroleum reservoir and groundwater aquifer simulation. The physical, geological, and chemical properties of the medium may lead to a degeneracy in the spatially varying diffusion coefficient of the mathematical equations describing the model.

Classical numerical methods exhibit instability in the solution even in the non-degenerate case, when the diffusion coefficient is sufficiently small compared to the advection coefficient. In such a situation, the ratio of advection to diffusion is sufficiently high to impose hyperbolic-type behavior in the solution and the numerical solution is incapable of capturing the resulting boundary layer phenomenon. Consequently, even though sufficient regularity exists in the mathematical description of the problem to expect stable results, the numerical scheme is unable to recognize the existence of small and possibly zero diffusion leading to extreme numerical instabilities. Although this phenomena may be resolved by refinement of the mesh, there is a corresponding considerable increase in computational effort.

Advection-diffusion equations of this type have been discretized using classical finite element and finite difference methods that typically utilize an operator splitting technique to handle the difficulties associated with advective transport and

Received by the editors July 2, 2008 and, in revised form, February 9, 2009.
The second author is grateful for the NSF support through the grants NSF DMS 0506039 and NSF DMS 0810422.

diffusion separately [23, 16]. Such computational methods often utilize slope limiting procedures to supress the amount of unphysical oscillations in the numerical solution or the inclusion of a streamline-diffusion stabilization term [15]. Additionally, domain decomposition techniques utilizing differing numerical methods on distinct subdomains have been proposed to model the multi-physics aspects of the problem [12, 25]. In this paper, we propose an adaptive flux technique to maintain stability, based on a discontinuous Galerkin (DG) discretization, that minimizes the L^2 norm of the error and makes the use of slope limiting techniques superfluous.

DG methods possess several characteristics which render them useful in many applications. The flexibility of the method allows for element-wise polynomial degree approximation and general non-conforming meshes. Some well known versions applied to elliptic equations include the symmetric interior penalty method (SIPG) [2], the OBB method [3], the non-symmetric interior penalty Galerkin method (NIPG) [20] and the incomplete interior penalty version (IIPG) [8]. In [14], the analysis is extended to advection-diffusion-reaction problems with variable tensor-valued diffusion but the proposed technique still exhibits the same instabilities as the classically defined DG methods we consider herein. DG methods have been applied to transport equations [19, 24] where the estimates derived are semi-discrete and present numerical examples for constant diffusion only. Alternative DG methods based on the discretization of hyperbolic equations include the local discontinous Galerkin method [6], subsequently extended by various authors to advection-diffusion equations.

The case of a spatially dependent, possibly degenerate diffusion coefficient has not been analyzed previously in the context of DG methods. In this work, our focus is to improve the numerical results in the case of a small (and possibly degenerate) diffusion coefficient without resorting to the use of slope-limiters nor the considerable increase in computational cost associated with mesh refinement. Under the assumption that the mesh fits the discontinuities of the diffusion coefficient, our scheme successfully detects the difficult boundary layer region and adaptively switches techniques to maintain stability. The boundary layer region occurs when the advection-diffusion ratio is sufficiently high that the method cannot resolve the small scale solution behavior. Instead, it treats the problem as the degenerate diffusion case where sufficient mathematical regularity does not exist to justify use of the SIPG/NIPG method. Indeed, the use of an averaged flux is only valid in the case of a continuous solution, which is not mathematically accurate in the degenerate diffusion case at the interface from low to high diffusivity. Only when the advection-diffusion ratio is relatively small can the original numerical technique recognize the small scale phenomena, i.e. non-degenerate diffusion. Our adaptive method automatically recognizes these regions of numerical instability and successfully produces an accurate, stable, and relatively efficient solution.

Verification is the process of demonstrating that a computational model accurately approximates the exact solution to a mathematical model. The identification and quantification of errors in the corresponding numerical implementation is a central component of this process [1, 22]. Our paper deals with verification in the sense that we show that the standard DG methods yield poor L^2 accurary with respect to benchmark solutions. We propose new adaptive DG methods that solve the mathematical model problem accurately. Moreover, our verification analysis is valid for a spatially varying diffusion coefficient that may possibly be degenerate. We obtain theoretical estimates for the L^2 norm of the error and we show numerically that our proposed method yields a smaller error.

In the following section, we define the formulation of our semi-discrete scheme. Error estimates are proved in Section 3. Both implicit and explicit fully discrete schemes are analysed in Section 4. Section 5 contains the adaptive scheme and corresponding analysis. Finally numerical examples are presented in Section 6.

2. Formulation

The specific equation we consider is of advection-diffusion type defined on a bounded polygonal domain Ω in $\mathbb{R}^n$, $n = 1, 2, 3$,

$$\partial_t u + \nabla \cdot (\beta u - \epsilon \nabla u) = f, \qquad \text{in} \quad \Omega \times (0, T), \tag{2}$$

supplemented with boundary and initial conditions

$$u(x,t) = u_0(x), \qquad x \in \Omega, t = 0, \tag{3}$$

$$(\beta u(x,t) - \epsilon \nabla u(x,t)) \cdot n_{\partial\Omega} = \beta u_{\text{in}} \cdot n_{\partial\Omega}, \qquad x \in \partial\Omega_{\text{in}},\ t \geq 0, \tag{4}$$

$$-\epsilon \nabla u(x,t) \cdot n_{\partial\Omega} = 0, \qquad x \in \partial\Omega_{\text{out}},\ t \geq 0, \tag{5}$$

where $u_0 \in L^2(\Omega)$ and $u_{\text{in}} \in L^2(\partial\Omega_{\text{in}})$. We assume that the velocity β is divergence-free: $\nabla \cdot \beta = 0$. Define inflow and outflow regions $\partial\Omega_{\text{in}} = \{x \in \partial\Omega : \beta \cdot n_{\partial\Omega} < 0\}$ and $\partial\Omega_{\text{out}} = \{x \in \partial\Omega : \beta \cdot n_{\partial\Omega} \geq 0\}$ respectively. The unit vector $n_{\partial\Omega}$ is outward to the boundary $\partial\Omega$.

We assume that the domain Ω is partitioned into two polygonal subdomains Ω_H and Ω_P. We assume that the spatially dependent function $\epsilon = \epsilon(x)$ is bounded in Ω uniformly: $0 \leq \epsilon_* \leq \epsilon \leq \epsilon^*$. In general, ϵ may vary over the domain with several orders of magnitude. However we assume that ϵ takes small values in the region Ω_H (for example $\epsilon = \mathcal{O}(10^{-4})$) and that ϵ takes larger values in the region Ω_P (for example $\epsilon = \mathcal{O}(1)$). For readibility, we denote $\epsilon_H = \epsilon|_{\Omega_H}$ and $\epsilon_P = \epsilon|_{\Omega_P}$. Let Γ define the interface between Ω_P and Ω_H. Conventionally set the unit normal n_Γ on Γ to face outward from Ω_{P} and inward to Ω_{H}. Define Γ_{HP} to be the subset of Γ through which the flow crosses from hyperbolic solution behavior (small diffusion coefficient) to parabolic solution behavior subdomains:

$$\Gamma_{\text{HP}} = \{x \in \Gamma : \beta \cdot n_\Gamma < 0\}.$$

The accuracy of the numerical solution at this interface Γ_{HP} from low to high diffusivity (and not vice-versa) is of primary interest, since the numerical solution may exhibit instability resulting in overshoot at this location.

Continuity of the total flux (ie the solution and the flux) must hold everywhere throughout the domain; however, in the limiting case where $\epsilon = 0$ on Ω_H, only the flux is continuous on the subset Γ_{HP} [13, 17]. Although the flow is continuous elsewhere in the domain, at this interface there is a discontinuity in the solution. Even in the case where diffusion is nonzero but small, the numerical solution mimics this limiting case and may exhibit overshoot on Γ_{HP} [10]. Consequently, we discretize the advection-diffusion equation via DG interior penalty techniqes and explore strategies for defining stable numerical flux functions on Γ_{HP}.

Let $\mathcal{T}_h = \{\Omega_e\}_e$ be a nondegenerate shape-regular subdivision of Ω such that Γ_{HP} is the union of a subset of edges in 2D (and faces in 3D). In other words, an element Ω_e is either a subset of Ω_H or a subset of Ω_P. As usual, we denote h_e to be the diameter of element Ω_e and h the maximum diameter of elements in $\mathcal{T}_h$. Let F_h be the set of faces belonging to elements $\Omega_e \in \mathcal{T}_h$ and partition F_h into distinct sets $F^i_{\text{HP}} \cup F^i \cup F^\partial_{\text{in}} \cup F^\partial_{\text{out}}$, where F^i_{HP} denotes the set of interior faces on interface region Γ_{HP}, F^i denotes the set of remaining interior faces, F^∂_{in} the set of faces located on $\partial\Omega_{\text{in}}$, and F^∂_{out} the set of faces located on $\partial\Omega_{\text{out}}$. To each face $F \in F_h$, we associate

a unit normal vector n_F such that n_F coincides with $n_{\partial\Omega}$ on $F^{\partial}_{\text{in}} \cup F^{\partial}_{\text{out}}$ and with n_Γ on F^i_{HP}. Let Δ_H denote the set of elements $\Omega_e \subset \Omega_H$ such that the intersection $\partial\Omega_e \cap F^i_{\text{HP}}$ contains at least one edge (or face). Define

$$\epsilon^{\Delta}_H = \max_{x\in\Delta_H} \epsilon_H(x).$$

Let p be a positive integer. Define the finite element approximating space

$$V_h = \{v_h \in L^2(\Omega) : \forall \Omega_e \in \mathcal{T}_h(\Omega), v_h|_{\Omega_e} \in \mathbb{P}^p(\Omega_e)\},$$

where $\mathbb{P}^p(\Omega_e)$ is the set of polynomials of total degree less than or equal to p. Let $(\cdot,\cdot)_{\Omega_e}$ and $\langle\cdot,\cdot\rangle_F$ denote the L^2 inner-product over $\Omega_e \in \mathcal{T}_h$ and $F \in F_h$ respectively. The corresponding L^2 norm is denoted by $\|\cdot\|_{\Omega_e}$ or $\|\cdot\|_F$. Let $H^k(\Omega)$ be the standard Sobolev space with norm $\|\cdot\|_{H^k(\Omega)}$ and semi-norm $|\cdot|_{H^k(\Omega)}$. Let $H^k(\mathcal{T}_h)$ be the broken Sobolev space.

$$H^k(\mathcal{T}_h) = \{v \in L^2(\Omega) : \forall \Omega_e \in \mathcal{T}_h(\Omega), v|_{\Omega_e} \in H^k(\Omega_e)\},$$

with norm $\|\cdot\|_{H^k(\mathcal{T}_h)} = (\sum_{\Omega_e\in\mathcal{T}_h} \|\cdot\|^2_{H^k(\Omega_e)})^{1/2}$. Let $L^2(0,T;H^k(\mathcal{T}_h))$ denote the space of functions v with $\int_0^T \|v(t)\|^2_{H^k(\mathcal{T}_h)} < \infty$. For any interior face $F = \partial\Omega_{e_1} \cap \partial\Omega_{e_2}$ with n_F pointing from Ω_{e_1} to Ω_{e_2}, we define the jump $[\cdot]$ and average operators $\{\cdot\}$:

$$\forall v_h \in V_h, \quad [v_h] = v_h|_{\Omega_{e_1}} - v_h|_{\Omega_{e_2}}, \quad \{v_h\} = 0.5(v_h|_{\Omega_{e_1}} + v_h|_{\Omega_{e_2}}).$$

We also define upwind and downwind quantities, using characteristic functions $1_{\{\cdot\}}$:

(6)
$$v^{\uparrow}_F = v|_{\Omega_{e_1}} 1_{\{\beta\cdot n_F \geq 0\}} + v|_{\Omega_{e_2}} 1_{\{\beta\cdot n_F<0\}}, \quad v^{\downarrow}_F = v|_{\Omega_{e_1}} 1_{\{\beta\cdot n_F<0\}} + v|_{\Omega_{e_2}} 1_{\{\beta\cdot n_F\geq 0\}}.$$

For $u_h, v_h \in V_h$, define the bilinear form

$$\begin{aligned} A(u_h,v_h) = &- \sum_{\Omega_e\in\mathcal{T}_h} (\beta u_h - \epsilon\nabla u_h, \nabla v_h)_{\Omega_e} + \sum_{F\in F^i} |F|^{-1}\langle\sigma_F[u_h],[v_h]\rangle_F \\ &+ \sum_{F\in F^i} \langle\beta u^{\uparrow}_h\cdot n_F,[v_h]\rangle_F + \sum_{F\in F^{\partial}_{\text{out}}} \langle\beta u_h\cdot n_F, v_h\rangle_F \\ &- \sum_{F\in F^i} \langle\{\epsilon\nabla u_h\}\cdot n_F,[v_h]\rangle_F + \kappa\sum_{F\in F^i}\langle\{\epsilon\nabla v_h\}\cdot n_F,[u_h]\rangle_F \\ &+ a(u_h,v_h) + d(u_h,v_h), \end{aligned} \tag{7}$$

and linear form

$$L(v_h) = (f,v_h)_\Omega - \sum_{F\in F^{\partial}_{\text{in}}} \langle\beta u_{\text{in}}\cdot n_F, v_h\rangle_F. \tag{8}$$

The coefficient κ takes the values: $\kappa \in \{+1,-1,0\}$, which yields respectively the non-symmetric, symmetric and incomplete interior penalty Galerkin method (except on the interface Γ_{HP}). The penalty parameter σ_F may vary from face to face, but for simplicity of writing we might drop the subscript F and use the notation σ. We will choose σ to be equal to 1 if $\kappa = 1$ (non-symmetric case) and bounded below by a large enough constant σ_0 if $\kappa = -1$ (symmetric case) (see [11]) or if $\kappa = 0$. Here, $|F|$ denotes the $(d-1)$-dimensional measure of F.

One aim of this paper is to study numerically and theoretically different approaches for defining the advective $a(\cdot,\cdot)$ and diffusive $d(\cdot,\cdot)$ fluxes on Γ_{HP}. In [18], we explore the results obtained by upwinding, averaging and downwinding the advective term and show numerically that, as expected, stable and accurate solutions

are obtained only for the case of upwinding. Consequently, we fix the advective interface flux to be upwinded:

$$a(u_h, v_h) = \sum_{F \in F^i_{\mathrm{HP}}} \langle (\beta u_h)^{\uparrow} \cdot n_F, [v_h] \rangle_F, \tag{9}$$

and consider the following numerical fluxes for the diffusion:

$$\begin{aligned} d(u_h, v_h) &= d_\nu(u_h, v_h) = -\nu(u_h, v_h) + \tilde{\kappa}\nu(v_h, u_h) + j_{\tilde{\sigma}_\nu}(u_h, v_h), \\ d(u_h, v_h) &= d_\alpha(u_h, v_h) = -\alpha(u_h, v_h) + \tilde{\kappa}\alpha(v_h, u_h) + j_{\tilde{\sigma}_\alpha}(u_h, v_h), \end{aligned}$$

where we have

$$\begin{aligned} \nu(u_h, v_h) &= \sum_{F \in F^i_{\mathrm{HP}}} \langle (\epsilon \nabla u_h)^{\uparrow} \cdot n_F, [v_h] \rangle_F, \\ \alpha(u_h, v_h) &= \sum_{F \in F^i_{\mathrm{HP}}} \langle \{\epsilon \nabla u_h\} \cdot n_F, [v_h] \rangle_F, \\ j_{\tilde{\sigma}}(u_h, v_h) &= \sum_{F \in F^i_{\mathrm{HP}}} |F|^{-1} \langle \tilde{\sigma}[u_h], [v_h] \rangle_F. \end{aligned}$$

In this paper, we refer as the *improved* DG method the case where $d = d_\nu$. If $\kappa = \sigma_F = \tilde{\kappa} = 1$ and $\tilde{\sigma}_\nu = \epsilon_H$, then the method is called *improved NIPG*. If $\kappa = \tilde{\kappa} = -1$ (resp. 0) with σ_F and $\tilde{\sigma}_\nu$ large enough, the method is called *improved SIPG* (resp. *improved IIPG*). We show that the improved DG method is convergent and yields a minimal L^2 error in space if there is an abrupt and substantial jump in the diffusivity coefficient.

In the general case where the diffusivity coefficient varies over a wide range of values, the proposed method is called *adaptive DG method* and it consists of a linear combination of the improved fluxes d_ν and the averaged fluxes d_α. To be more precise, the adaptive DG method uses the following flux on F^i_{HP}:

$$\begin{aligned} d_\theta(u_h, v_h) = &\sum_{F \in F^i_{\mathrm{HP}}} \langle -(1-\theta)(\epsilon \nabla u_h)^{\uparrow} \cdot n_F + (1-\theta)|F|^{-1}\tilde{\sigma}_\nu [u_h], [v_h] \rangle_F \\ + &\sum_{F \in F^i_{\mathrm{HP}}} \langle \tilde{\kappa}(1-\theta)(\epsilon \nabla v_h)^{\uparrow} \cdot n_F, [u_h] \rangle_F + \sum_{F \in F^i_{\mathrm{HP}}} \langle -\theta\{\epsilon \nabla u_h\} \cdot n_F + \theta |F|^{-1} \tilde{\sigma}_{\tilde{\alpha}} [u_h], [v_h] \rangle_F \\ &+ \sum_{F \in F^i_{\mathrm{HP}}} \langle \tilde{\kappa}\theta\{\epsilon \nabla v_h\} \cdot n_F, [u_h] \rangle_F \end{aligned} \tag{10}$$

where θ is the function varying in space, defined by:

$$\forall x \in \Gamma_{\mathrm{HP}}, \quad \theta(x) = \frac{\epsilon_H(x)}{\epsilon_P(x)}.$$

This adaptive flux automatically detects the appropriate amount of upwinding versus averaging. We show in Section 5 that the adaptive DG method is convergent and that it minimizes the L^2 norm of the error in space for varying diffusivity coefficients.

We recall that the choice d_α corresponds to the standard interior penalty Galerkin flux (see [19]) if $\tilde{\sigma}_\alpha$ is nonzero (symmetric if $\tilde{\kappa} = -1$, non-symmetric if $\tilde{\kappa} = 1$) and to the IIPG flux if $\tilde{\kappa} = 0$. If both $\tilde{\sigma}_\alpha$ and $\tilde{\kappa}$ are zero, the case $d = d_\alpha$ is simply an averaged diffusive flux without any additional terms. In [18] we have explored various choices of fluxes.

For any $t > 0$, the continuous in time solution $u_h(t) \in V_h$ of (2) satifies

$$\forall v_h \in V_h, \quad (\partial_t u_h, v_h)_\Omega + A(u_h(t), v_h) = L(v_h), \tag{11}$$

$$\forall v_h \in V_h, \quad (u_h(0), v_h)_\Omega = (u_0, v_h)_\Omega. \tag{12}$$

Our investigation of various flux functions defined on Γ_{HP} is motivated by the numerical instabilities of the computed solution when the diffusion coefficient on Ω_H is very small. In the limiting case $\epsilon = 0$ on Ω_H, the interface conditions are relatively well understood. In [13], a vanishing viscosity singular perturbation analysis is employed to derive appropriate theoretical interface conditions: continuity of the flux must hold across any hyperbolic and parabolic interface, whereas continuity of the solution is not satisfied on the subset Γ_{HP}. We remark that these interface conditions were used in [7] to establish well-posedness of a one dimensional periodic degenerate diffusion advection-diffusion equation. These conditions were numerically verified in [10] where it is shown that for a non-vanishing but small ϵ_H, the modified NIPG method with flux $d = 0$ yields a stable solution without overshoot whereas the standard NIPG method produces an incorrect solution.

To better motivate our work, we present a numerical example indicative of the numerical difficulties associated with small diffusivities. The coarse mesh is defined in Fig. 1 with gray areas indicating Ω_H and white areas Ω_P. We consider the case $\beta = (1, 0), \epsilon_P = 1$ and $\epsilon_H = 10^{-3}$. The problem is described in detail in Section 6.1. Fig. 2 (left) shows the "exact" solution, which is in fact an overkill solution obtained on a very fine mesh. The standard NIPG solution obtained on the coarse mesh is shown in Fig. 2 (middle); this solution clearly exhibits large amount of overshoot near the interface Γ_{HP}. Fig. 2 (right) shows our proposed adaptive flux solution on the coarse mesh which is almost identical to that of the exact solution. All three solutions are for linear basis functions and explicit time discretization.

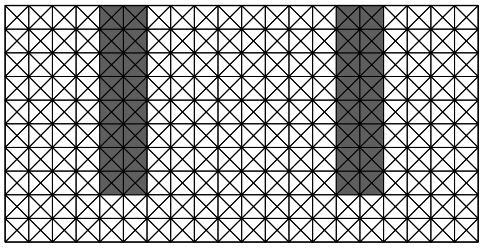

FIGURE 1. Mesh and domain partition of hyperbolic-type subdomains where $\epsilon_H = 10^{-3}$ (gray) and parabolic-type subdomain where $\epsilon_P = 1$ (white).

3. Analysis

In this section we analyze the DG scheme (11)-(12) with the improved and averaged diffusive fluxes $d = d_\nu, d_\alpha$. We prove stability bounds, then state the consistency of the scheme and derive error estimates in the L^2 norm. We first define one condition that may be assumed to hold for certain values of $\tilde{\kappa}$, $\tilde{\sigma}_\alpha$ and $\tilde{\sigma}_\nu$.

Condition I: The penalty parameters $\tilde{\sigma}_\nu$ and $\tilde{\sigma}_\alpha$ are equal to a sufficiently large enough constant $\tilde{\sigma}_0$.

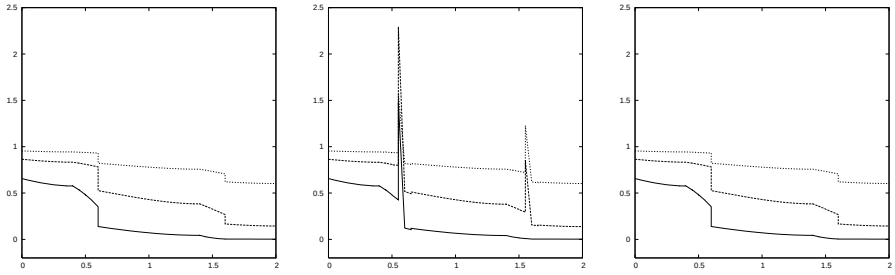

FIGURE 2. "Exact" overkill solution (left), standard explicit NIPG solution ($d = d_\alpha$ and $\kappa = \sigma_F = \tilde{\kappa} = \tilde{\sigma}_\alpha = 1$) (middle) and adaptive NIPG solution ($d = d_\theta$ with $\kappa = \sigma_F = \tilde{\kappa} = \tilde{\sigma}_\alpha = 1$ and $\tilde{\sigma}_\nu = \epsilon_H$ (right) at times t_0 (solid line), t_1 (dashed line) and t_2 (dotted line).

Let us define the norm $|||\cdot|||_{\tilde{\sigma}}$:

$$|||v_h|||_{\tilde{\sigma}}^2 = \sum_{\Omega_e \in \mathcal{T}_h} \|\epsilon^{1/2}\nabla v_h\|_{\Omega_e}^2 + \sum_{F \in F^i \cup F^i_{\mathrm{HP}}} \||\beta \cdot n_F|^{1/2}[v_h]\|_F^2$$

$$+ \sum_{F \in F^\partial_{\mathrm{in}} \cup F^\partial_{\mathrm{out}}} \||\beta \cdot n_F|^{1/2} v_h\|_F^2 + \sum_{F \in F^i} |F|^{-1}\|\sigma_F^{1/2}[v_h]\|_F^2 + j_{\tilde{\sigma}}(v_h, v_h). \tag{13}$$

In the definition above, it is understood that $\tilde{\sigma}$ is equal to $\tilde{\sigma}_\nu$ for the choice $d = d_\nu$ and $\tilde{\sigma}_\alpha$ for the choice $d = d_\alpha$. The notation $\tilde{\sigma}$ will be used for readability provided there is no confusion.

3.1. Analysis Tools. In subsequent analysis, we will use the following trace inequalities with respect to $h_e = \mathrm{diam}(\Omega_e)$ [2]:

$$\forall v \in H^1(\Omega_e), \quad \|v\|_F^2 \le C_t\Big(\frac{1}{h_e}\|v\|_{\Omega_e}^2 + h_e|v|_{H^1(\Omega_e)}^2\Big), \tag{14}$$

$$\forall v \in H^2(\Omega_e), \quad \|\nabla v \cdot n_F\|_F^2 \le C_t\Big(\frac{1}{h_e}|v|_{H^1(\Omega_e)}^2 + h_e|v|_{H^2(\Omega_e)}^2\Big). \tag{15}$$

For polynomial functions, we use the following trace lemma [21]:

Lemma 3.1. *For element Ω_e in $\mathbb{R}^n$, $(n = 2, 3)$ with $h_e = \mathrm{diam}(\Omega_e)$, let F be an edge or a face of Ω_e with unit normal vector n_F. Then, if v_h is a polynomial on Ω_e, there exists a constant C_τ independent of Ω_e such that*

$$\|v_h\|_F \le C_\tau h_e^{-1/2}\|v_h\|_{\Omega_e}, \tag{16}$$

$$\|\nabla v_h \cdot n_F\|_F \le C_\tau h_e^{-1/2}\|\nabla v_h\|_{\Omega_e}. \tag{17}$$

Recall the standard inverse inequality [4, 9]: there exists a constant C_i independent of Ω_e such that for any v_h polynomial on Ω_e

$$\|v_h\|_{H^1(\Omega_e)} \le C_i h_e^{-1}\|v_h\|_{\Omega_e}. \tag{18}$$

We will have occasion to use a function $u^*(t) \in V_h$ that satisfies the following approximation properties: For $q = 0, 1, 2$,

$$\forall t \in (0, T), \quad \forall \Omega_e, \quad \|u(t) - u^*(t)\|_{H^q(\Omega_e)} \le C_a h^{p+1-q}|u(t)|_{H^{p+1}(\Omega_e)}. \tag{19}$$

$$\forall t \in (0, T), \quad \forall \Omega_e, \quad \|\partial_t u(t) - \partial_t u^*(t)\|_{\Omega_e} \le C_a h^p|\partial_t u(t)|_{H^p(\Omega_e)}. \tag{20}$$

Finally, we will use the constant C throughout the paper for a generic constant independent of h and ϵ, unless specified otherwise. We will also explicitly add to the constant the parameters on which this constant depends: for instance, the constant $C_{i,\tau,\sigma}$ depends on C_i, C_τ, and σ.

3.2. Stability and Consistency. In this section, we derive stability bounds for the proposed schemes and determine consistency.

Theorem 3.2. *Let u_h be the semi-discrete solution in V_h to (11)-(12). Then u_h satisfies the bound:*

(21)
$$\|u_h(T)\|_\Omega^2+\int_0^T |||u_h(t)|||_{\tilde\sigma}^2 dt \leq \|u_h(0)\|_\Omega^2+C_{\tau,\epsilon^*}\int_0^T (\|f\|_\Omega^2+\sum_{F\in F_{\rm in}^\partial} \||\beta\cdot n_F|^{1/2}u_{\rm in}\|_F^2)dt,$$

where C_{τ,ϵ^*} is a constant independent of h and ϵ_* but dependent on C_τ and ϵ^*. This stability bound holds unconditionally except in the cases $\tilde\kappa \in \{-1,0\}$ where Condition I is needed.

Proof. Fix $t>0$. To simplify notation, we write $u_h(t)=u_h$. Using Green's formula and the fact that $\nabla\cdot\beta=0$, we have [5]:

$$-\sum_{\Omega_e\in\mathcal{T}_h}(\beta u_h,\nabla u_h)_{\Omega_e}=-\langle\beta\cdot n_{\partial\Omega},\frac{1}{2}u_h^2\rangle_{\partial\Omega}-\sum_{F\in F^i\cup F_{\rm HP}^i}\langle\beta\cdot n_F,\frac{1}{2}[u_h^2]\rangle_F.$$

Thus taking $v_h=u_h$ in (11) yields:

$$\begin{aligned}\frac{1}{2}\frac{d}{dt}\|u_h\|_\Omega^2+\sum_{\Omega_e\in\mathcal{T}_h}\|\epsilon^{1/2}\nabla u_h\|_{\Omega_e}^2+\frac{1}{2}\sum_{F\in F^i\cup F_{\rm HP}^i}\||\beta\cdot n_F|^{1/2}[u_h]\|_F^2\\ +\frac{1}{2}\sum_{F\in F_{\rm in}^\partial\cup F_{\rm out}^\partial}\||\beta\cdot n_F|^{1/2}u_h\|_F^2+\sum_{F\in F^i}|F|^{-1}\|\sigma_F^{1/2}[u_h]\|_F^2\\ -(1-\kappa)\sum_{F\in F^i}\langle\{\epsilon\nabla u_h\cdot n_F\},[u_h]\rangle_F+d(u_h,u_h)=L(u_h).\end{aligned}\tag{22}$$

Using Young's inequality, we bound $L(u_h)$:

$$|L(u_h)|\leq\frac{1}{4}\sum_{F\in F_{\rm in}^\partial}\||\beta\cdot n_F|^{1/2}u_h\|_F^2+\sum_{F\in F_{\rm in}^\partial}\||\beta\cdot n_F|^{1/2}u_{\rm in}\|_F^2+\frac{1}{4}\|f\|_\Omega^2+\|u_h\|_\Omega^2,$$

and the equation (22) becomes:

$$\begin{aligned}\frac{1}{2}\frac{d}{dt}\|u_h\|_\Omega^2+\sum_{\Omega_e\in\mathcal{T}_h}\|\epsilon^{1/2}\nabla u_h\|_{\Omega_e}^2+\frac{1}{2}\sum_{F\in F^i\cup F_{\rm HP}^i}\||\beta\cdot n_F|^{1/2}[u_h]\|_F^2\\ +\frac{1}{2}\sum_{F\in F_{\rm out}^\partial}\||\beta\cdot n_F|^{1/2}u_h\|_F^2+\frac{1}{4}\sum_{F\in F_{\rm in}^\partial}\||\beta\cdot n_F|^{1/2}u_h\|_F^2\\ +\sum_{F\in F^i}|F|^{-1}\|\sigma_F^{1/2}[u_h]\|_F^2+d(u_h,u_h)\leq\sum_{F\in F_{\rm in}^\partial}\||\beta\cdot n_F|^{1/2}u_{\rm in}\|_F^2+\frac{1}{4}\|f\|_\Omega^2+\|u_h\|_\Omega^2\\ +|(1-\kappa)\sum_{F\in F_{\rm HP}^i}\langle\{\epsilon\nabla u_h\cdot n_F\},[u_h]\rangle_F|.\end{aligned}\tag{23}$$

Let us first assume that $\kappa = 1$ in (7). It remains to bound the diffusive flux term $d(u_h, u_h)$. In the case where $\tilde{\kappa} = 1$, we have $d_\nu = d_\alpha = j_{\tilde{\sigma}}$, and this yields

$$\frac{d}{dt}\|u_h\|_\Omega^2 + |||u_h|||_{\tilde{\sigma}}^2 \leq \sum_{F\in F_{\text{in}}^\partial} \||\beta\cdot n_F|^{1/2}u_{\text{in}}\|_F^2 + \frac{1}{4}\|f\|_\Omega^2 + \|u_h\|_\Omega^2. \tag{24}$$

We conclude by integrating from 0 to T and using Gronwall's lemma.
For $\tilde{\kappa} = 0$, we have $d_\nu = -\nu + j_{\tilde{\sigma}}$ and $d_\alpha = -\alpha + j_{\tilde{\sigma}}$. In the first case, the term $\nu(u_h, u_h)$ is bounded by using the definition of the jump term:

$$|\nu(u_h, u_h)| \leq C_\tau \epsilon_H \sum_{F\in F_{\text{HP}}^i} |F|^{-1/2}\|[u_h]\|_F^2 + \frac{1}{4}\sum_{\Omega_e\in\Delta_H} \|\epsilon^{1/2}\nabla u_h\|_{\Omega_e}^2.$$

Thus, both terms can be hidden in the left-hand side of the equation (23) if $\tilde{\sigma} \geq C_\tau\epsilon_H$. In other words, we obtain (21) if Condition I holds true. Finally, in the second case, the following bound is obtained using trace inequality Lemma (3.1):

$$\alpha(u_h, u_h) \leq \frac{1}{2}\sum_{\Omega_e\in\mathcal{T}_h} \|\epsilon^{1/2}\nabla u_h\|_{\Omega_e}^2 + C_{\tau,\epsilon^*}\sum_{F\in F_{\text{HP}}^i} |F|^{-1}\|[u_h]\|_F^2. \tag{25}$$

Thus, (23) becomes

$$\begin{aligned}
&\frac{1}{2}\frac{d}{dt}\|u_h\|_\Omega^2 + \frac{1}{2}\sum_{\Omega_e\in\mathcal{T}_h}\|\epsilon^{1/2}\nabla u_h\|_{\Omega_e}^2 + \frac{1}{2}\sum_{F\in F^i\cup F_{\text{HP}}^i} \||\beta\cdot n_F|^{1/2}[u_h]\|_F^2 \\
&+\frac{1}{2}\sum_{F\in F_{\text{out}}^\partial} \||\beta\cdot n_F|^{1/2}u_h\|_F^2 + \frac{1}{4}\sum_{F\in F_{\text{in}}^\partial} \||\beta\cdot n_F|^{1/2}u_h\|_F^2 + \sum_{F\in F^i} |F|^{-1}\|\sigma_F^{1/2}[u_h]\|_F^2 \\
&+(\tilde{\sigma} - C_{\tau,\epsilon^*})\sum_{F\in F_{\text{HP}}^i} |F|^{-1}\|[u_h]\|_F^2 \leq \sum_{F\in F_{\text{in}}^\partial} \||\beta\cdot n_F|^{1/2}u_{\text{in}}\|_F^2 + \|f\|_\Omega^2 + \|u_h\|_\Omega^2.
\end{aligned}$$

Then, Condition I, integration from 0 to T and Gronwall's lemma yield the stability bound. Finally, in the case $\tilde{\kappa} = -1$, the diffusive fluxes are $d_\nu = -2\nu + j_{\tilde{\sigma}}$ and $d_\alpha = -2\alpha + j_{\tilde{\sigma}}$. It is clear that as above, Condition I is needed for $d = d_\nu$ and for $d = d_\alpha$. The case $\kappa = 1$ and $\kappa = -1$ are handled similarly if σ is bounded below by a large enough constant.

Remark 3.3. *Existence and uniqueness of the solution of (11) is a corollary of the stability result Theorem 3.2 and the theory of ordinary differential equations.*

For the consistency of the scheme, we see that the solution u of (2) satisfies:

$$\forall v_h \in V_h, \quad (\frac{\partial u}{\partial t}, v_h) + A(u, v_h) = L(v_h). \tag{26}$$

3.3. Semi-Discrete Error Analysis. We next derive a semi-discrete a priori error estimate in the energy norm.

Theorem 3.4. *For $t > 0$, let $u_h(t)$ be the semi-discrete solution in V_h to (11)-(12). Assume that $u_0 \in H^{p+1}(\mathcal{T}_h)$, $u \in L^2(0,T;H^{p+1}(\mathcal{T}_h))$ and $\partial_t u \in L^2(0,T;H^p(\mathcal{T}_h))$. Then there exists a constant $C_{i,\tau,t,\beta,a,\sigma,\epsilon^*}$ independent of h and ϵ_* such that*

$$\begin{aligned}
&\|(u-u_h)(T)\|_\Omega^2 + \int_0^T |||u(t)-u_h(t)|||_{\tilde{\sigma}}^2 dt \leq \\
&C_{i,\tau,t,\beta,a,\sigma,\epsilon^*}\, h^{2p}\Big(|u_0|_{H^{p+1}(\mathcal{T}_h)}^2 + \int_0^T |u(t)|_{H^{p+1}(\mathcal{T}_h)}^2 dt + \int_0^T |\partial_t u(t)|_{H^p(\mathcal{T}_h)}^2 dt\Big),
\end{aligned} \tag{27}$$

for the following cases:

- $d = d_\nu, \tilde{\kappa} = 1$. *Note that the constant depends on* $\tilde{\sigma}_0^{-1}$ *if* $\tilde{\sigma}_\nu = \tilde{\sigma}_0$. *If* $\tilde{\sigma}_\nu = 1$ *or* $\tilde{\sigma}_\nu = \epsilon_H$, *the constant is independent of* $\tilde{\sigma}_\nu$.
- $d = d_\nu, \tilde{\kappa} \in \{-1, 0\}$, $\tilde{\sigma}_\nu = 1$ *and* $\sqrt{\epsilon_H^\Delta}$ *small enough.*
- $d = d_\nu, \tilde{\kappa} \in \{-1, 0\}$, $\tilde{\sigma}_\nu = \tilde{\sigma}_0$ *and Condition I. The constant depends on* $\tilde{\sigma}_0^{-1}$.
- $d = d_\nu, \tilde{\kappa} \in \{-1, 0\}$, $\tilde{\sigma}_\nu = \epsilon_H$ *under the condition* $0 \leq \sqrt{\epsilon_H^\Delta} < h$.
- $d = d_\alpha, \tilde{\kappa} = 1, \tilde{\sigma}_\alpha \in \{1, \tilde{\sigma}_0\}$. *The constant depends on* $\tilde{\sigma}_0^{-1}$ *if* $\tilde{\sigma}_\alpha = \tilde{\sigma}_0$.
- $d = d_\alpha, \tilde{\kappa} \in \{-1, 0\}$ *and* $\tilde{\sigma}_\alpha = \tilde{\sigma}_0$ *and Condition I. The constant depends on* $\tilde{\sigma}_0^{-1}$ *if* $\tilde{\sigma}_\alpha = \tilde{\sigma}_0$.

The estimate is

$$\|(u - u_h)(T)\|_\Omega^2 + \int_0^T |||u(t) - u_h(t)|||_{\tilde{\sigma}}^2 dt \leq$$

(28)

$$C_{i,\tau,t,\beta,a,\sigma,\epsilon^*} h^{2p} \Big(|u_0|^2_{H^{p+1}(\mathcal{T}_h)} + (1 + \frac{\epsilon^*}{\min\limits_{x \in \Delta_H} \epsilon_H(x)}) \int_0^T |u(t)|^2_{H^{p+1}(\mathcal{T}_h)} dt + \int_0^T |\partial_t u(t)|^2_{H^p(\mathcal{T}_h)} dt \Big)$$

for the choice $d = d_\alpha, \quad \tilde{\kappa} = 1, \quad \tilde{\sigma}_\alpha = \epsilon_H$.

Proof. Subtracting (26) from (11) gives the error equation:

$$(\partial_t(u_h - u), v_h)_\Omega - \sum_{\Omega_e \in \mathcal{T}_h} (\beta(u_h - u) - \epsilon \nabla(u_h - u), \nabla v_h)_{\Omega_e} + d(u_h - u, v_h)$$

$$+ \sum_{F \in F^i \cup F^i_{\mathrm{HP}}} \langle \beta(u_h - u)^\uparrow \cdot n_F, [v_h] \rangle_F - \sum_{F \in F^i} \langle \{\epsilon \nabla(u_h - u) \cdot n_F\}, [v_h] \rangle_F + \sum_{F \in F^\partial_{\mathrm{out}}} \langle \beta(u_h - u), v_h \rangle_F$$

$$+\kappa \sum_{F \in F^i} \langle \{\epsilon \nabla v_h \cdot n_F\}, [u_h - u] \rangle_F + \sum_{F \in F^i} |F|^{-1} \langle \sigma_F [u_h - u], [v_h] \rangle_F = 0. \tag{29}$$

We decompose the error $u_h - u = \eta - \xi$ with $\eta = u_h - u^*$ and $\xi = u - u^*$, with u^* satisfying (19)-(20). Then, choosing $v_h = \eta$ in the error equation (29) yields:

$$\frac{1}{2} \frac{d}{dt} \|\eta\|_\Omega^2 + \sum_{\Omega_e \in \mathcal{T}_h} \|\epsilon^{1/2} \nabla \eta\|^2_{\Omega_e} + \sum_{F \in F^i} |F|^{-1} \|\sigma_F^{1/2}[\eta]\|_F^2$$

$$+ \frac{1}{2} \sum_{F \in F^i \cup F^i_{\mathrm{HP}}} \| |\beta \cdot n_F|^{1/2} [\eta] \|_F^2 + \frac{1}{2} \sum_{F \in F^\partial_{\mathrm{in}} \cup F^\partial_{\mathrm{out}}} \| |\beta \cdot n_F|^{1/2} \eta \|_F^2$$

$$= (\partial_t \xi, \eta)_\Omega - \sum_{\Omega_e \in \mathcal{T}_h} (\beta \xi, \nabla \eta)_{\Omega_e} + \sum_{\Omega_e \in \mathcal{T}_h} (\epsilon \nabla \xi, \nabla \eta)_{\Omega_e} + \sum_{F \in F^i \cup F^i_{\mathrm{HP}}} \langle \beta \xi^\uparrow \cdot n_F, [\eta] \rangle_F$$

$$- \sum_{F \in F^i} \langle \{\epsilon \nabla \xi \cdot n_F\}, [\eta] \rangle_F + \kappa \sum_{F \in F^i} \langle \{\epsilon \nabla \eta \cdot n_F\}, [\xi] \rangle_F + \sum_{F \in F^i} |F|^{-1} \langle \sigma_F [\xi], [\eta] \rangle_F$$

$$+ \sum_{F \in F^\partial_{\mathrm{out}}} \langle \beta \xi \cdot n_F, \eta \rangle_F - (1 - \kappa) \sum_{F \in F^i} \langle \{\epsilon \nabla \eta \cdot n_F\}, [\eta] \rangle_F + d(\xi, \eta) - d(\eta, \eta)$$

$$= T_1 + \cdots + T_{11}. \tag{30}$$

We now briefly bound the first nine terms. The techniques used are standard to the discontinuous Galerkin methods. The first term T_1 is easily bounded by Cauchy-Schwarz and Young's inequalities:

$$T_1 \leq \frac{1}{2} \|\eta\|_\Omega^2 + \frac{1}{2} \|\partial_t \xi\|_\Omega^2.$$

Using inverse inequality (18), the second term is bounded as

$$T_2 \leq \frac{1}{2}\|\eta\|_\Omega^2 + C_i h^{-2}\frac{1}{2}\|\beta\|_\infty^2\|\xi\|_\Omega^2. \tag{31}$$

Similarly the term T_3 is bounded

$$T_3 \leq \frac{1}{16}\sum_{\Omega_e\in\mathcal{T}_h}\|\epsilon^{1/2}\nabla\eta\|_{\Omega_e}^2 + 4\epsilon^*\|\nabla\xi\|_\Omega^2. \tag{32}$$

For the fourth term we have:

$$T_4 \leq \frac{1}{16}\sum_{F\in F^i\cup F^i_{\mathrm{HP}}}\||\beta\cdot n_F|^{1/2}[\eta]\|_F^2 + 4\|\beta\|_\infty\sum_{F\in F^i\cup F^i_{\mathrm{HP}}}\|\xi^\uparrow\|_F^2. \tag{33}$$

We have for T_5

$$T_5 \leq \frac{1}{16}\sum_{F\in F^i}|F|^{-1}\|\sigma_F^{1/2}[\eta]\|_F^2 + \epsilon^* h\sum_{F\in F^i}\sigma_F^{-1}\|\{\nabla\xi\cdot n_F\}\|_F^2, \tag{34}$$

and for T_6:

$$T_6 \leq \frac{1}{16}\sum_{\Omega_e\in\mathcal{T}_h}\|\epsilon^{1/2}\nabla\eta\|_{\Omega_e}^2 + C_{\tau,\epsilon^*}\sum_{F\in F^i}|F|^{-1}\|[\xi]\|_F^2. \tag{35}$$

The term T_7 is easily bounded as

$$T_7 \leq \frac{1}{16}\sum_{F\in F^i}|F|^{-1}\|\sigma_F^{1/2}[\eta]\|_F^2 + 4\sum_{F\in F^i}|F|^{-1}\|\sigma_F^{1/2}[\xi]\|_F^2. \tag{36}$$

The term T_8 is bounded similar to T_4:

$$T_8 \leq \frac{1}{16}\sum_{F\in F^\partial_{\mathrm{out}}}\||\beta\cdot n_F|^{1/2}\eta\|_F^2 + 4\|\beta\|_\infty\sum_{F\in F^\partial_{\mathrm{out}}}\|\xi\|_F^2.$$

If $\kappa = 1$, the term T_9 vanishes. Otherwise, we use a similar argument as in (25) using Lemma (3.1):

$$T_9 \leq \frac{1}{8}\sum_{\Omega_e\in\mathcal{T}_h}\|\epsilon^{1/2}\nabla\eta\|_{\Omega_e}^2 + C_{\tau,\epsilon^*}\sum_{F\in F^i_{\mathrm{HP}}}|F|^{-1}\|[\eta]\|_F^2. \tag{37}$$

Combining the bounds above, for $\kappa = 1$, equation (30) becomes:

$$\frac{1}{2}\frac{d}{dt}\|\eta\|_\Omega^2 + \frac{3}{4}\sum_{\Omega_e\in\mathcal{T}_h}\|\epsilon^{1/2}\nabla\eta\|_{\Omega_e}^2 + \frac{7}{8}\sum_{F\in F^i}|F|^{-1}\|\sigma_F^{1/2}[\eta]\|_F^2$$

$$+\frac{7}{16}\sum_{F\in F^i\cup F^i_{\mathrm{HP}}}\||\beta\cdot n_F|^{1/2}[\eta]\|_F^2 + \frac{1}{2}\sum_{F\in F^\partial_{\mathrm{in}}}\||\beta\cdot n_F|^{1/2}\eta\|_F^2 + \frac{7}{16}\sum_{F\in F^\partial_{\mathrm{out}}}\||\beta\cdot n_F|^{1/2}\eta\|_F^2$$

$$\leq \|\eta\|_\Omega^2 + C_{i,\tau,t,\beta,a,\sigma,\epsilon^*}\,h^{2p}(|u|^2_{H^{p+1}(\mathcal{T}_h)} + |\partial_t u|^2_{H^p(\mathcal{T}_h)}) + d(\xi,\eta) - d(\eta,\eta). \tag{38}$$

If $\kappa = -1$, the resulting equation differs from (38) only by the constant in front of $\sum_{F\in F^i}|F|^{-1}\|\sigma_F^{1/2}[\eta]\|_F^2$. We will now continue the analysis of the scheme by considering each diffusive flux on Γ_{HP} separately.

Case $d = d_\nu$: We first consider the numerical flux $d = d_\nu$ with $\tilde{\kappa} = 1$. The last two terms of (38) are:

$$T_{10} + T_{11} = -\nu(\xi,\eta) - j_{\tilde{\sigma}}(\eta,\eta).$$

The first term is bounded as follows:

$$-\nu(\xi,\eta) \leq C_{t,a,\epsilon^*}\, h^{2p}|u|^2_{H^{p+1}(\mathcal{T}_h)} + \frac{1}{16} j_{\tilde{\sigma}}(\eta,\eta), \quad \text{if} \quad \tilde{\sigma} = 1, \epsilon_H,$$

or as follows:

$$-\nu(\xi,\eta) \leq C_{t,a,\epsilon^*,\tilde{\sigma}^{-1}}\, h^{2p}|u|^2_{H^{p+1}(\mathcal{T}_h)} + \frac{1}{16} j_{\tilde{\sigma}}(\eta,\eta), \quad \text{if} \quad \tilde{\sigma} = \tilde{\sigma}_0,$$

and the second term can be hidden in the left-hand side of (38). Thus, we obtain the estimate:

(39)

$$\|\eta(t)\|^2_\Omega + \int_0^t |||\eta|||^2_{\tilde{\sigma}} \leq \|\eta(0)\|^2_\Omega + C_{i,\tau,\beta,\epsilon^*,a}\, h^{2p}\Big(\int_0^t |u|^2_{H^{p+1}(\mathcal{T}_h)} + \int_0^t |\partial_t u|^2_{H^p(\mathcal{T}_h)}\Big),$$

with the constant depending on $\tilde{\sigma}^{-1}$ if $\tilde{\sigma} = \tilde{\sigma}_0$. If $\tilde{\kappa} \in \{-1, 0\}$, we need to bound the additional term $-\nu(\eta,\eta)$. First, if $\tilde{\sigma} = \tilde{\sigma}_0$ we have:

$$\sum_{F\in F^i_{\mathrm{HP}}} \langle (\epsilon\nabla\eta)^\uparrow \cdot n_F, [\eta]\rangle_F \leq \frac{1}{32} \sum_{\Omega_e\in\Delta_H} \|\epsilon^{1/2}\nabla\eta\|^2_{\Omega_e} + C_\tau \epsilon^\Delta_H \sum_{F\in F^i_{\mathrm{HP}}} |F|^{-1}\|[\eta]\|^2_F. \tag{40}$$

Provided $\tilde{\sigma}_0$ is large enough, both terms can be hidden in the left-hand side of (38). The estimate is then (39). If $\tilde{\sigma} = 1$, we have

$$\sum_{F\in F^i_{\mathrm{HP}}} \langle (\epsilon\nabla\eta)^\uparrow \cdot n_F, [\eta]\rangle_F \leq \frac{1}{32} \sum_{\Omega_e\in\Delta_H} \|\epsilon^{1/2}\nabla\eta\|^2_{\Omega_e} + C_\tau \epsilon^\Delta_H j_{\tilde{\sigma}}(\eta,\eta).$$

Both terms can be hidden in the left-hand side of (38) if $C_\tau \epsilon^\Delta_H < 1$. The estimate is still (39). Finally if $\tilde{\sigma} = \epsilon_H$, we have:

$$T_{11} = (1-\tilde{\kappa})\nu(\eta,\eta) \leq C_\tau \|\eta\|^2_\Omega + \epsilon^\Delta_H h^{-2} \sum_{\Omega_e\in\Delta_H} \|\epsilon^{1/2}\nabla\eta\|^2_{\Omega_e}. \tag{41}$$

Therefore, using the condition $0 \leq \sqrt{\epsilon^\Delta_H} < h$, we have (39).

Case $d = d_\alpha$: Next, if $d = d_\alpha$, the last two terms in (38) are:

$$T_{10} + T_{11} = -\alpha(\xi,\eta) + (1-\tilde{\kappa})\alpha(\eta,\eta) - j_{\tilde{\sigma}}(\eta,\eta).$$

If $\tilde{\kappa} = 1$ and $\tilde{\sigma} \in \{1, \tilde{\sigma}_0\}$, then we easily obtain the estimate (39) using the bound:

$$\alpha(\xi,\eta) \leq C_{t,\tilde{\sigma},\epsilon^*,a}\, h^{2p}|u|^2_{H^{p+1}(\mathcal{T}_h)} + \frac{1}{32} \sum_{F\in F^i_{\mathrm{HP}}} |F|^{-1}\|\tilde{\sigma}^{1/2}[\eta]\|^2_F. \tag{42}$$

If $\tilde{\sigma} = \epsilon_H$, then we have

$$\alpha(\xi,\eta) \leq \frac{1}{32} j_{\tilde{\sigma}}(\eta,\eta) + C_{t,a} \frac{\epsilon^*}{\min_{x\in\Delta_H} \epsilon(x)} h^{2p}|u|^2_{H^{p+1}(\mathcal{T}_h)}, \tag{43}$$

which yields the estimate (28). Finally, the additional term to bound in the case $\tilde{\kappa} \in \{-1, 0\}$ is

$$\alpha(\eta,\eta) \leq \frac{1}{32} \sum_{\Omega_e\in\mathcal{T}_h} \|\epsilon^{1/2}\nabla\eta\|^2_F + C_{\tau,\epsilon^*} \sum_{F\in F^i_{\mathrm{HP}}} |F|^{-1}\|[\eta]\|^2_F, \tag{44}$$

which can be subtracted from the left-hand side of (38) if $\tilde{\sigma}_0$ is large enough.

A simple corollary of Theorem 3.4 is the convergence of the method in particular cases.

Lemma 3.5. *Let u_h be solution of (11) with d chosen as one of the following*

- $d(u_h, v_h) = -\nu(u_h, v_h) + \nu(v_h, u_h) + j_{\tilde{\sigma}_\nu}(u_h, v_h)$
- $d(u_h, v_h) = -\nu(u_h, v_h) - \nu(v_h, u_h) + j_{\tilde{\sigma}_\nu}(u_h, v_h)$ *with* $\tilde{\sigma}_\nu = \tilde{\sigma}_0$ *large enough.*
- $d(u_h, v_h) = -\nu(u_h, v_h) + j_{\tilde{\sigma}_\nu}(u_h, v_h)$ *with* $\tilde{\sigma}_\nu = \tilde{\sigma}_0$ *large enough.*
- $d(u_h, v_h) = -\alpha(u_h, v_h) + \alpha(v_h, u_h) + j_{\tilde{\sigma}_\alpha}(u_h, v_h)$ *with* $\tilde{\sigma}_\alpha = 1$.
- $d(u_h, v_h) = -\alpha(u_h, v_h) - \alpha(v_h, u_h) + j_{\tilde{\sigma}_\alpha}(u_h, v_h)$ *with* $\tilde{\sigma}_\alpha = \tilde{\sigma}_0$ *large enough.*
- $d(u_h, v_h) = -\alpha(u_h, v_h) + j_{\tilde{\sigma}_\alpha}(u_h, v_h)$ *with* $\tilde{\sigma}_\alpha = \tilde{\sigma}_0$ *large enough.*

Then, the numerical error in the energy norm and in the L^2 norm converges to zero. The rates are optimal for the energy norm, namely $\mathcal{O}(h^p)$.

We now conclude this section with a few remarks.

Remark 3.6. *One can show* [18] *that for the case $d = 0$, the error estimate is:*

$$\|(u-u_h)(T)\|_\Omega^2 + \int_0^T |||u(t)-u_h(t)|||_0^2 dt \leq C_t(\epsilon_H^\Delta h^{-1})^2 \int_0^T \|u\|_{H^2(\mathcal{T}_h)}^2$$

(45)

$$+C_{i,\tau,t,\beta,a,\sigma,\epsilon^*} h^{2p}\Big(|u_0|_{H^{p+1}(\mathcal{T}_h)}^2 + \int_0^T |u(t)|_{H^{p+1}(\mathcal{T}_h)}^2 dt + \int_0^T |\partial_t u(t)|_{H^p(\mathcal{T}_h)}^2 dt\Big)$$

Therefore, it is possible to have an accurate solution on a given mesh if $\epsilon_H^\Delta \leq h^{p+1}$, but this method does not converge as the mesh size tends to zero.

Remark 3.7. *In general, the analysis is valid for degenerate $\epsilon_H = 0$, except in the case $d = d_\alpha, \tilde{\kappa} = 1$ and $\tilde{\sigma}_\alpha = \epsilon_H$. In addition no assumption on the relative size of ϵ_H with respect to ϵ_P is made.*

Remark 3.8. *Error estimates cannot be obtained for the case $d = d_\alpha$, $\tilde{\kappa} \in \{-1, 0\}$ and $\tilde{\sigma}_\alpha \in \{1, \epsilon_H\}$.*

4. Fully Discrete Scheme and Analysis

Let Δt be a positive time step and let $t^j = j\Delta t$ denote the time at the j^{th} step. We denote by v^j the function v evaluated at time t^j. We define the linear form $L^{j+1} : V_h \to \mathbb{R}$:

$$L^{j+1}(v_h) = (f^{j+1}, v_h)_\Omega - \sum_{F \in F_{\text{in}}^\partial} \langle \beta u_{\text{in}}^{j+1} \cdot n_F, v_h \rangle_F. \tag{46}$$

4.1. Backward Euler time discretization. In this paper, we refer to the implicit DG solution as the solution defined by:

$$\forall v_h \in V_h, \quad (\frac{u_h^{j+1} - u_h^j}{\Delta t}, v_h) + A(u_h^{j+1}, v_h) = L^{j+1}(v_h), \tag{47}$$

$$\forall v_h \in V_h, \quad (u_h^0, v_h) = (u_0, v_h). \tag{48}$$

We first derive a stability bound then present an error estimate:

Theorem 4.1. *For $t > 0$, let $(u_h^j)_j$ be the discrete solution in V_h to (47)-(48). If $\tilde{\kappa} \in \{-1, 0\}$ and either $d = d_\alpha$ or $d = d_\nu$, assume that Condition I holds true. Then, there is $\Delta t_0 > 0$ such that for all $\Delta t \leq \Delta t_0$, $(u_h^j)_j$ satisfies the bound for all $n > 0$:*

$$\|u_h^n\|_\Omega^2 + C\Delta t \sum_{j=1}^n |||u_h^j|||_{\tilde{\sigma}}^2 dt \leq \|u_0\|_\Omega^2 + C_{\tau,\epsilon^*}\Delta t \sum_{j=1}^n (\|f^j\|_\Omega^2 + \sum_{F \in F_{\text{in}}^\partial} \||\beta \cdot n_F|^{1/2} u_{\text{in}}^j\|_F^2),$$

where C_{τ,ϵ^*} is a constant independent of $h, \Delta t$ and ϵ_*.

Proof. Choose $v_h = u_h^{j+1}$ in (47). We obtain a similar bound as in (23):

$$\frac{1}{2\Delta t}(\|u_h^{j+1}\|_\Omega^2 - \|u_h^j\|_\Omega^2) + \sum_{\Omega_e\in\mathcal{T}_h} \|\epsilon^{1/2}\nabla u_h^{j+1}\|_{\Omega_e}^2 + \frac{1}{2}\sum_{F\in F^i\cup F^i_{\rm HP}} \||\beta\cdot n_F|^{1/2}[u_h^{j+1}]\|_F^2$$
$$+\frac{1}{2}\sum_{F\in F^\partial_{\rm out}} \||\beta\cdot n_F|^{1/2}u_h^{j+1}\|_F^2 + \frac{1}{4}\sum_{F\in F^\partial_{\rm in}} \||\beta\cdot n_F|^{1/2}u_h^{j+1}\|_F^2$$
$$+\sum_{F\in F^i}|F|^{-1}\|\sigma_F^{1/2}[u_h^{j+1}]\|_F^2 + d(u_h^{j+1},u_h^{j+1}) \le \sum_{F\in F^\partial_{\rm in}} \||\beta\cdot n_F|^{1/2}u_{\rm in}^{j+1}\|_F^2 + \frac{1}{4}\|f^{j+1}\|_\Omega^2$$
$$+\|u_h^{j+1}\|_\Omega^2 + |(1-\kappa)\sum_{F\in F^i_{\rm HP}}\langle\{\epsilon\nabla u_h^{j+1}\cdot n_F\},[u_h^{j+1}]\rangle_F|.$$

Using similar arguments as in the proof of Theorem 3.2, we obtain:

$$\frac{1}{2\Delta t}(\|u_h^{j+1}\|_\Omega^2 - \|u_h^j\|_\Omega^2) + C|||u_h^{j+1}|||_{\tilde\sigma}^2$$
$$\le C_\tau\|u_h^{j+1}\|_\Omega^2 + C_{\tau,\epsilon^*}(\sum_{F\in F^\partial_{\rm in}} \||\beta\cdot n_F|^{1/2}u_{\rm in}^{j+1}\|_F^2 + \|f^{j+1}\|_\Omega^2), \tag{49}$$

We then multiply the inequality by $2\Delta t$ and sum over $j = 0,\dots,n-1$:

$$(1-2C_\tau\Delta t)\|u_h^n\|_\Omega^2 - \|u_h^0\|_\Omega^2 + 2C\Delta t\sum_{j=1}^n |||u_h^j|||_{\tilde\sigma}^2$$
$$\le 2C_\tau\Delta t\sum_{j=1}^{n-1}\|u_h^j\|_\Omega^2 + 2C_{\tau,\epsilon^*}\Delta t\sum_{j=1}^n(\sum_{F\in F^\partial_{\rm in}} \||\beta\cdot n_F|^{1/2}u_{\rm in}^j\|_F^2 + \|f^j\|_\Omega^2)$$

Under the assumption that $1-2C_\tau\Delta t > 0$ and using a discrete Gronwall's estimate, we obtain the final result.

We then remark that the exact solution u satisfies:

$$\forall v_h\in V_h,\quad (\frac{\partial u}{\partial t}(t^{j+1}),v_h) + A(u^{j+1},v_h) = L^{j+1}(v_h). \tag{50}$$

Theorem 4.2. *Let u be the solution of (2)-(5) and let $(u_h^j)_j \in V_h$ be the sequence of discrete solutions satisfying (47)-(48). Assume that $u_0 \in H^{p+1}(\mathcal{T}_h)$, $u \in L^2(0,T;H^{p+1}(\mathcal{T}_h))$ and $\partial_t u, \partial_{tt}u \in L^2(0,T;H^p(\mathcal{T}_h))$. There is a constant $\Delta t_0 > 0$ such that for all $\Delta t < \Delta t_0$, and constants $C, C_{i,\tau,t,\beta,a,\sigma,\epsilon^*}$ independent of h, and ϵ_* such that*

$$\|u^n - u_h^n\|_\Omega^2 + \Delta t\sum_{j=1}^n |||u^j - u_h^j|||_{\tilde\sigma}^2 \le C\Delta t^2\int_0^T \|\partial_{tt}u(t)\|_\Omega^2 dt$$
$$+C_{i,\tau,t,\beta,a,\sigma,\epsilon^*}\,h^{2p}\Big(|u_0|^2_{H^{p+1}(\mathcal{T}_h)} + \Delta t\sum_{j=1}^n |u^j|^2_{H^{p+1}(\mathcal{T}_h)} + \Delta t\sum_{j=1}^n |\partial_t u^j|^2_{H^p(\mathcal{T}_h)}\Big), \tag{51}$$

for the following cases:

- $d = d_\nu, \tilde\kappa = 1$. *The constant also depends on $\tilde\sigma_\nu^{-1}$ if $\tilde\sigma_\nu = \tilde\sigma_0$.*
- $d = d_\nu, \tilde\kappa \in \{-1,0\}$, $\tilde\sigma_\nu = 1$ *and* $\sqrt{\epsilon_H^\Delta}$ *small enough.*
- $d = d_\nu, \tilde\kappa \in \{-1,0\}$, $\tilde\sigma_\nu = \tilde\sigma_0$ *and Condition I.*
- $d = d_\nu, \tilde\kappa \in \{-1,0\}$, $\tilde\sigma_\nu = \epsilon_H$ *and under the condition* $0 \le \sqrt{\epsilon_H^\Delta} < h$.
- $d = d_\alpha, \tilde\kappa = 1, \tilde\sigma_\alpha \in \{1,\tilde\sigma_0\}$. *The constant also depends on $\tilde\sigma_\alpha^{-1}$ if $\tilde\sigma_\alpha = \tilde\sigma_0$.*

- $d = d_\alpha, \tilde{\kappa} \in \{-1, 0\}$ *and* $\tilde{\sigma}_\alpha = \tilde{\sigma}_0$ *and Condition I. The constant also depends on* $\tilde{\sigma}_\alpha^{-1}$ *if* $\tilde{\sigma}_\alpha = \tilde{\sigma}_0$.

The estimate is

$$\|u^n - u_h^n\|_\Omega^2 + \Delta t \sum_{j=1}^{n} |||u^j - u_h^j|||_{\tilde{\sigma}}^2 \leq C\Delta t^2 \int_0^T \|\partial_{tt} u(t)\|_\Omega^2 dt$$

$$+C_{i,\tau,t,\beta,a,\sigma,\epsilon^*} h^{2p} \Big(|u_0|_{H^{p+1}(\mathcal{T}_h)}^2 + (1 + \frac{\epsilon^*}{\min\limits_{x\in\Delta_H} \epsilon_H(x)}) \int_0^T |u(t)|_{H^{p+1}(\mathcal{T}_h)}^2 dt + \int_0^T |\partial_t u(t)|_{H^p(\mathcal{T}_h)}^2 dt \Big),$$

for the case $d = d_\alpha, \quad \tilde{\kappa} = 1, \quad \tilde{\sigma}_\alpha = \epsilon_H$.

Proof. Using the same notation as in the proof of Theorem 3.4, we have from subtracting (50) from (47) and choosing $v_h = \eta^{j+1}$:

$$\begin{aligned}
&\frac{1}{2\Delta t}(\|\eta^{j+1}\|_\Omega^2 - \|\eta^j\|_\Omega^2) + \sum_{\Omega_e \in \mathcal{T}_h} \|\epsilon^{1/2} \nabla \eta^{j+1}\|_{\Omega_e}^2 + \sum_{F \in F^i} |F|^{-1} \|\sigma_F^{1/2} [\eta^{j+1}]\|_F^2 \\
&\quad + \frac{1}{2} \sum_{F \in F^i \cup F_{\mathrm{HP}}^i} \||\beta \cdot n_F|^{1/2} [\eta^{j+1}]\|_F^2 + \frac{1}{2} \sum_{F \in F_{\mathrm{in}}^\partial \cup F_{\mathrm{out}}^\partial} \||\beta \cdot n_F|^{1/2} \eta^{j+1}\|_F^2 \\
&= (\partial_t u^*(t^{j+1}) - \frac{u^{*j+1} - u^{*j}}{\Delta t}, \eta^{j+1})_\Omega + (\partial_t \xi(t^{j+1}), \eta^{j+1})_\Omega - \sum_{\Omega_e \in \mathcal{T}_h} (\beta \xi^{j+1}, \nabla \eta^{j+1})_{\Omega_e} \\
&\quad + \sum_{\Omega_e \in \mathcal{T}_h} (\epsilon \nabla \xi^{j+1}, \nabla \eta^{j+1})_{\Omega_e} + \sum_{F \in F^i \cup F_{\mathrm{HP}}^i} \langle \beta \xi^{\uparrow, j+1} \cdot n_F, [\eta^{j+1}] \rangle_F \\
&\quad - \sum_{F \in F^i} \langle \{\epsilon \nabla \xi^{j+1} \cdot n_F\}, [\eta^{j+1}] \rangle_F + \kappa \sum_{F \in F^i} \langle \{\epsilon \nabla \eta^{j+1} \cdot n_F\}, [\xi^{j+1}] \rangle_F \\
&\quad + \sum_{F \in F_{\mathrm{out}}^\partial} \langle \beta \xi^{j+1} \cdot n_F, \eta^{j+1} \rangle_F - (1 - \kappa) \sum_{F \in F^i} \langle \{\epsilon \nabla \eta^{j+1} \cdot n_F\}, [\eta^{j+1}] \rangle_F \\
&\quad + \sum_{F \in F^i} |F|^{-1} \langle \sigma_F [\xi^{j+1}], [\eta^{j+1}] \rangle_F + d(\xi^{j+1}, \eta^{j+1}) - d(\eta^{j+1}, \eta^{j+1}). \qquad (52)
\end{aligned}$$

As the remainder of the proof is similar to the proof of Theorem 3.4, we only present the bounds for the first two terms in the right-hand side of (52). Using a Taylor expansion with integral remainder, we have

$$\begin{aligned}
\|\partial_t u^*(t^{j+1}) - \frac{u^{*j+1} - u^{*j}}{\Delta t}\|_\Omega^2 &\leq \frac{1}{2\Delta t^2} \int_{t^j}^{t^{j+1}} (s - t^j)^2 ds \int_{t^j}^{t^{j+1}} \|\partial_{tt} u^*\|_\Omega^2 \\
&\leq \frac{\Delta t}{6} \int_{t^j}^{t^{j+1}} \|\partial_{tt} u^*\|_\Omega^2. \qquad (53)
\end{aligned}$$

Therefore, we have

$$(\partial_t u^*(t^{j+1}) - \frac{u^{*j+1} - u^{*j}}{\Delta t}, \eta^{j+1})_\Omega \leq \|\eta^{j+1}\|_\Omega^2 + C\Delta t^3 \int_{t^j}^{t^{j+1}} \|\partial_{tt} u^*\|_\Omega^2.$$

The second term in the right-hand side of (52) is bounded as

$$(\partial_t \xi(t^{j+1}), \eta^{j+1})_\Omega \leq \|\eta^{j+1}\|_\Omega^2 + C_a\, h^{2p} |\partial_t u^{j+1}|_{H^p(\mathcal{T}_h)}^2.$$

As in the derivation of the stability result, we need the time step to be small enough in order to conclude. A discrete Gronwall's lemma is used, and the rest of the proof is straightforward.

Remark 4.3. *Except in the case* $d = d_\nu, \tilde{\kappa} \in \{-1, 0\}, \tilde{\sigma}_\nu = \epsilon_H$, *we can replace the constraint "*Δt *small enough" by the constraint* $\epsilon_* > 0$. *The constant* C *in the right-hand side of the resulting estimate will then additionally depend on* $1/\epsilon_*$.

4.2. Forward Euler time discretization. In this paper, we refer to the explicit DG solution as the solution defined by:

$$\forall v_h \in V_h, \quad (\frac{u_h^{j+1} - u_h^j}{\Delta t}, v_h) = L^j(v_h) - A(u_h^j, v_h), \tag{54}$$

$$\forall v_h \in V_h, \quad (u_h^0, v_h) = (u_0, v_h). \tag{55}$$

To derive stability and an error estimate for the forward Euler discretization, we will assume throughout this section that the triangulation is quasi-uniform. Inverse inequality (18) yields the following result.

Lemma 4.4. *There is a constant* $C_b = C_{\epsilon^*, i, \beta, \tau}$ *independent of* h *and* ϵ_* *such that*

$$\forall v_h, w_h \in V_h, \quad A(v_h, w_h) \leq C_b\, h^{-1} \|v_h\|_\Omega |||w_h|||_0. \tag{56}$$

Theorem 4.5. *For* $t > 0$, *let* $(u_h^j)_j$ *be the discrete solution in* V_h *to (54)-(55). If* $d = d_\alpha$ *and* $\tilde{\kappa} \in \{-1, 0\}$, *assume that Condition I holds true. Assume that Condition I holds true for* $d = d_\nu$ *and* $\tilde{\kappa} \in \{-1, 0\}$. *Then, there is a constant* C_0 *independent of* h *and* ϵ_* *such that if* $\Delta t \leq C_0$ *and* $h^{-2}\Delta t \leq C_0$, *there is a constant* C_b *independent of* h *and* ϵ_* *such that* $(u_h^j)_j$ *satisfies the bound for all* $n > 0$*:*

$$\|u_h^n\|_\Omega^2 + C\Delta t \sum_{j=1}^n |||u_h^j|||_0^2 \leq \|u_0\|_\Omega^2 + C_b \Delta t \sum_{j=1}^n (\|f^j\|_\Omega^2 + \sum_{F \in F_{\text{in}}^\partial} \||\beta \cdot n_F|^{1/2} u_{\text{in}}^j\|_F^2).$$

Proof. Choose $v_h = u_h^{j+1}$ in (54). We obtain:

$$\begin{aligned}
&\frac{1}{2\Delta t}(\|u_h^{j+1}\|_\Omega^2 - \|u_h^j\|_\Omega^2 + \|u_h^j - u_h^{j+1}\|_\Omega^2) + A(u_h^{j+1}, u_h^{j+1}) = L^j(u_h^{j+1}) + A(u_h^{j+1} - u_h^j, u_h^{j+1}) \\
&\quad \leq \sum_{F \in F_{\text{in}}^\partial} \||\beta \cdot n_F|^{1/2} u_{\text{in}}^j\|_F^2 + \frac{1}{4}\|f^j\|_\Omega^2 + \frac{1}{4} \sum_{F \in F_{\text{in}}^\partial} \||\beta \cdot n_F|^{1/2} u_h^{j+1}\|_F^2 + \|u_h^{j+1}\|_\Omega^2 \\
&\qquad + C_b^2 h^{-2} \|u_h^j - u_h^{j+1}\|_\Omega^2 + \frac{1}{4}|||u_h^{j+1}|||^2.
\end{aligned}$$

We rewrite the term $A(u_h^{j+1}, u_h^{j+1})$ and obtain the following inequality:

$$\begin{aligned}
&\frac{1}{2\Delta t}(\|u_h^{j+1}\|_\Omega^2 - \|u_h^j\|_\Omega^2) + (\frac{1}{2\Delta t} - C_b^2 h^{-2})\|u_h^j - u_h^{j+1}\|_\Omega^2 \\
&+ \frac{3}{4} \sum_{\Omega_e \in \mathcal{T}_h} \|\epsilon^{1/2} \nabla u_h^{j+1}\|_{\Omega_e}^2 + \frac{1}{4} \sum_{F \in F^i \cup F_{\text{HP}}^i} \||\beta \cdot n_F|^{1/2} [u_h^{j+1}]\|_F^2 \\
&+ \frac{1}{4} \sum_{F \in F_{\text{out}}^\partial} \||\beta \cdot n_F|^{1/2} u_h^{j+1}\|_F^2 + \frac{3}{4} \sum_{F \in F^i} |F|^{-1} \|\sigma_F^{1/2} [u_h^{j+1}]\|_F^2 \\
+ d(u_h^{j+1}, u_h^{j+1}) &\leq \sum_{F \in F_{\text{in}}^\partial} \||\beta \cdot n_F|^{1/2} u_{\text{in}}^j\|_F^2 + \frac{1}{4}\|f^j\|_\Omega^2 + \|u_h^{j+1}\|_\Omega^2 + \frac{1}{4} j_{\tilde{\sigma}}(u_h^{j+1}, u_h^{j+1}) \\
&\quad + |(1 - \kappa) \sum_{F \in F^i} \langle \{\epsilon \nabla u_h^{j+1} \cdot n_F\}, [u_h^{j+1}] \rangle_F|.
\end{aligned}$$

The rest of the proof follows as in the case of backward Euler. Here, we have the additional stability condition (also called CFL condition):

$$\Delta t C_b^2 h^{-2} < \frac{1}{2}.$$

Theorem 4.6. *Let u be the solution of (2)-(5) and let $(u_h^j)_j \in V_h$ be the sequence of discrete solutions satisfying (54)-(55). Assume that $u_0 \in H^{p+1}(\mathcal{T}_h)$, $u \in L^\infty(0,T;H^{p+1}(\mathcal{T}_h))$ and $\partial_t u \in L^\infty(0,T;H^p(\mathcal{T}_h))$ and $\partial_{tt} u \in L^2((0,T)\times\Omega)$. There is a constant C_0 independent of h and ϵ_* such that if $\Delta t \le C_0$ and $h^{-2}\Delta t \le C_0$, then there are constants $C, C_{b,a}$ independent of h and ϵ_* such that*

$$\|u^n - u_h^n\|_\Omega^2 \le C\Delta t^2 \int_0^T \|\partial_{tt} u\|_\Omega^2$$
$$+C_{b,a} h^{2p}\Big(|u_0|^2_{H^{p+1}(\mathcal{T}_h)} + \Delta t \sum_{j=1}^{n-1} |u^j|^2_{H^{p+1}(\mathcal{T}_h)} + \Delta t \sum_{j=0}^{n-1} |\partial_t u^j|^2_{H^p(\mathcal{T}_h)}\Big).$$

Proof. Since the proof uses similar arguments as for the stability result and the proof for the convergence of the backward Euler scheme, we only give the first steps. We write the error equation as:

$$\frac{1}{2\Delta t}(\|\eta^{j+1}\|_\Omega^2 - \|\eta^j\|_\Omega^2 + \|\eta^{j+1}-\eta^j\|_\Omega^2) + A(\eta^j, \eta^{j+1}) = A(\eta^{j+1}-\eta^j, \eta^{j+1})$$
$$+A(\xi^j, \eta^{j+1}) + (\partial_t \xi(t^j), \eta^{j+1})_\Omega + (\partial_t u^*(t^j) - \frac{u^{*j+1}-u^{*j}}{\Delta t}, \eta^{j+1}).$$

We also have, as in (53):

$$\|\partial_t u^*(t^j) - \frac{u^{*j+1}-u^{*j}}{\Delta t}\|_\Omega^2 \le C\Delta t \int_{t^j}^{t^{j+1}} \|\partial_{tt} u^*\|_\Omega^2.$$

Furthermore, we have

$$A(\eta^{j+1}-\eta^j, \eta^{j+1}) \le \frac{1}{4}|||\eta^{j+1}|||^2 + C_b^2 h^{-2}\|\eta^{j+1}-\eta^j\|_\Omega^2.$$

Thus, it remains to bound the standard terms $A(\xi^j, \eta^{j+1})$ and $(\partial_t \xi(t^j), \eta^{j+1})_\Omega$. The remainder of the proof follows that of the backward Euler scheme.

5. Adaptive Fluxes

In this section, we analyze the adaptive method that uses on the interface Γ_{HP} the flux d_θ introduced in Section 2. This flux is obtained as a weighted average of the standard NIPG/SIPG fluxes and the upwind flux. When the interface region indicates a large difference between the diffusion coefficients, the scheme selects a stronger emphasis on the upwinding interface terms. Similarly, when there is less difference between the hyperbolic and parabolic coefficients, the scheme selects a stronger emphasis on the standard DG average flux definition. Our motivation for considering such an adaptive definition is highlighted in Section 6, where we demonstrate its excellent numerical results when applied to a domain with highly varying diffusion coefficient. Essentially, the use of an adaptive flux enables the scheme to automatically decide when to employ an upwinding strategy, in the case of advective to diffusive flow, versus a standard averaging technique everywhere else. In this way, the adaptive scheme successfully detects the difficult boundary layer region, and switches to an upwinding technique to maintain stability.

The parameters in the definition of d_θ are chosen to be:

- either $\tilde{\kappa} = 1$ with $\tilde{\sigma}_\nu = \epsilon_H$ and $\tilde{\sigma}_\alpha = 1$: the method is called *adaptive NIPG*.
- or $\tilde{\kappa} \in \{-1, 0\}$ and $\tilde{\sigma}_\nu = \tilde{\sigma}_\alpha = \tilde{\sigma}_0$ with $\tilde{\sigma}_0$ large enough: the method is called *adaptive SIPG* or *adaptive IIPG*.

With these definitions, the scheme (11) is unconditionally stable.

Theorem 5.1. *Assume that $d = d_\theta$ defined in (10). The solution u_h in V_h of (11)-(12) satisfies the following estimate:*

$$\|u_h(T)\|_\Omega^2 + \int_0^T |||u_h|||_0^2 + \int_0^T \sum_{F \in F_{\mathrm{HP}}^i} |F|^{-1} \|(\theta\tilde{\sigma}_\alpha + (1-\theta)\tilde{\sigma}_\nu)^{1/2}[u_h]\|_F^2$$
$$\leq \|u_h(0)\|_\Omega^2 + C_{\tau,\epsilon^*} \int_0^T \left(\|f\|_\Omega^2 + \sum_{F \in F_{\mathrm{in}}^\partial} \||\beta \cdot n_F|^{1/2} u_{\mathrm{in}}\|_F^2 \right),$$

where C_{τ,ϵ^*} is a constant independent of h and ϵ_* but dependent on C_τ and ϵ^* whenever $\tilde{\kappa} \neq 1$.

Proof. We obtain as in Theorem 3.2, the inequality (23). If $\tilde{\kappa} = 1$, then we obtain the bound:

$$\|u_h(T)\|_\Omega^2 + \int_0^T |||u_h|||_0^2 + \int_0^T \sum_{F \in F_{\mathrm{HP}}^i} |F|^{-1} \|(\theta + (1-\theta)\epsilon_H)^{1/2} u_h\|^2$$
$$\leq \|u_h(0)\|_\Omega^2 + C(\|f\|_\Omega^2 + \sum_{F \in F_{\mathrm{in}}^\partial} \||\beta \cdot n_F|^{1/2} u_{\mathrm{in}}\|_F^2). \tag{57}$$

The case $\tilde{\kappa} \in \{-1, 0\}$ is handled in a similar fashion; the bound (57) is derived assuming that $\tilde{\sigma}_0$ is large enough. The final estimate is obtained then by integrating in time and using Gronwall's lemma.

It is easy to see that the adaptive flux d_θ produces a consistent scheme. We next state some semi-discrete a priori error estimates. We skip the proof as it is similar to the proof of Theorem 3.4

Theorem 5.2. *Let u be the solution of (2)-(5) and for $t > 0$ let $u_h(t) \in V_h$ be the discrete solution of (11)-(12) with $d = d_\theta$. Assume that $u_0 \in H^{p+1}(\mathcal{T}_h)$, $u \in L^2(0, T; H^{p+1}(\mathcal{T}_h))$ and $\partial_t u \in L^2(0, T; H^p(\mathcal{T}_h))$. There is a constant $C_{i,\tau,t,\beta,a,\sigma,\epsilon^*}$ independent of h and ϵ such that*

$$\|(u - u_h)(T)\|_\Omega^2 + \int_0^T |||u(t) - u_h(t)|||_0^2 dt + \int_0^T \sum_{F \in F_{\mathrm{HP}}^i} \|(\theta\tilde{\sigma}_\alpha + (1-\theta)\tilde{\sigma}_\nu)^{1/2}[u(t) - u_h(t)]\|_F^2 dt$$
$$\leq C_{i,\tau,t,\beta,a,\sigma,\epsilon^*} h^{2p} \Big(|u_0|_{H^{p+1}(\mathcal{T}_h)}^2 + \int_0^t |u(t)|_{H^{p+1}(\mathcal{T}_h)}^2 dt + \int_0^t |\partial_t u(t)|_{H^p(\mathcal{T}_h)}^2 dt \Big),$$

The constant $C_{i,\tau,t,\beta,a,\sigma,\epsilon^*}$ also depends on $\tilde{\sigma}_0^{-1}$ if $\tilde{\sigma}_\alpha = \tilde{\sigma}_\nu = \tilde{\sigma}_0$ for the adaptive SIPG/IIPG methods.

Remark 5.3. *It is clear that we also obtain fully discrete estimates as in Section 4. If the time discretization is the backward Euler, then the stability bound of Theorem 4.1) holds and the error estimate (51) is valid.*

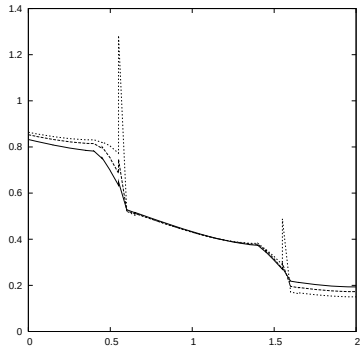

FIGURE 3. Varying diffusivity: standard NIPG solution everywhere for $\epsilon_H = 0.1$ (solid line), $\epsilon_H = 0.05$ (dashed line), and $\epsilon_H = 0.01$ (dotted line) in Ω_H at time $t_1 = 1.0$.

6. Numerical Experiments

6.1. Study of Fluxes. In this section, we investigate the numerical effect of the advective and diffusive fluxes listed in Section 2. We consider a simple test problem with large local Peclet number, which is inversely proportional to the diffusivity coefficient. Our domain is a two-dimensional rectangular region $[0, 2] \times [0, 1]$ with a triangular mesh consisting of 200 elements displayed in Fig. 1. We impose noflow conditions on top and bottom boundaries, an inflow value of $u_{\text{in}} = 1$ on the left boundary, and outflow on the right boundary. The initial solution consists of $u = 0$ everywhere in the domain. The velocity is $\beta = (1, 0)$ and the source function f is zero. Unless otherwise specified, the diffusion parameter is $\epsilon_P = 1$ on Ω_{P} and $\epsilon_H = 10^{-3}$ on Ω_{H}. The timestep is sufficiently small so that spatial error dominates the computation; hence our results are independent of the timestep size.

This particular test problem highlights the numerical difficulties encountered in modeling advection dominated regimes. For instance, Fig. 3 shows the numerical solution for various values of ϵ_H and a fixed mesh size. We focus on the profile of the numerical solution along $\{(x, 0.5) : 0 \le x \le 2\}$ obtained with the standard NIPG method everywhere ($d = d_\alpha$, $\kappa = \sigma_F = \tilde{\kappa} = \tilde{\sigma}_\alpha = 1$, $p = 1$) and a forward Euler scheme. If the ratio ϵ_H to ϵ_P is of order one, there are no instabilities. If the ratio is much smaller than one, then the instabilities increase at the interface from low to high diffusivity. One can see that the magnitude of these instabilities directly affect the L^2 norm of the error: the larger the instabilities, the higher the error norm. It is well known that the accuracy of the solution in advection dominated regimes can be improved by refining the mesh. However, a refinement in the computational mesh introduces a considerable computational cost that we aim to avoid while maintaining the integrity of the solution.

Next, in Fig. 4 we compare the effects of the time discretization technique on the numerical solution for the standard NIPG method defined everywhere ($d = d_\alpha$, $\kappa = \sigma_F = \tilde{\kappa} = \tilde{\sigma}_\alpha = 1$). The left figure shows the solution obtained by the forward Euler scheme, whereas the right two figures show the solution obtained by the backward Euler scheme. The time step is taken 20 times larger than for the forward Euler scheme. The implicit time discretization is more numerically diffusive. The overall amount of overshoot is reduced but still present. It is not surprising to observe that the overshoot phenomena are exacerbated when the polynomial degree is increased.

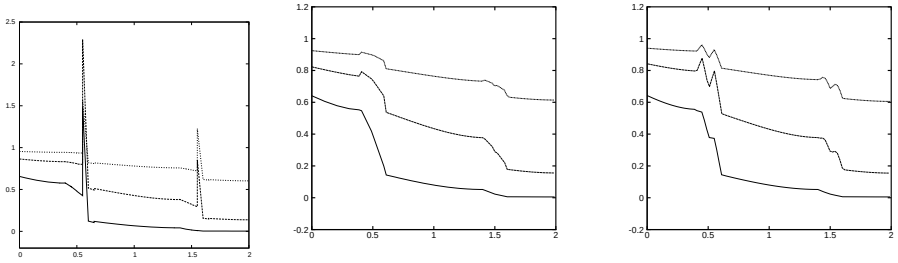

FIGURE 4. Time discretization comparison: standard NIPG solution: explicit $p = 1$ (left), implicit $p = 1$ (middle) and implicit $p = 2$ (right), at times t_0 (solid line), t_1 (dashed line) and t_2 (dotted line).

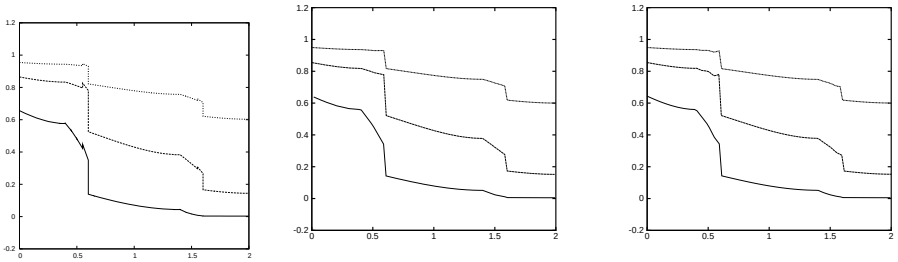

FIGURE 5. Time discretization comparison: improved NIPG solution: explicit $p = 1$ (left), implicit $p = 1$ (center) and implicit $p = 2$ (right), at times t_0 (solid line), t_1 (dashed line) and t_2 (dotted line).

We now explore various definitions of the flux at interface Γ_{HP}. The numerical solutions for the explicit discretization for $p = 1$ and implicit scheme for $p = 1, 2$ are shown in Fig. 5. The overshoots for the explicit time discretization are minimal, and they disappear for the implicit time discretization, even when the polynomial degree is increased.

We obtain less accurate results by retaining $d = d_\nu$ and further varying the values for the parameters $\tilde{\kappa}$ and $\tilde{\sigma}_\nu$. Results for the explicit time discretization are shown in Fig. 6, 7, 8. Clearly these solutions are not as accurate as those in Fig. 5, and the overshoots are greatest for the IIPG flux on Γ_{HP} (Fig. 8). For these tests, increasing the penalty value from 1 to 10 exacerbates the overshoot phenomena.

From the previous experiments, we conclude that the choice $d = d_\nu$ with $\tilde{\kappa} = 1$, $\tilde{\sigma}_\nu = \epsilon_H$ on Γ_{HP} yield the most accurate results for this particular example. We now choose the adaptive flux $d = d_\theta$. Fig. 9 shows the explicit solution for $p = 1$ and the implicit solution for $p = 1, 2$. The overshoot phenomena disappears for the implicit solution while the fronts remain sharp. We note that qualitatively, there is no noticeable difference between figures 5 and 9. However, in the next section we will compute quantitative values of the L^2 norm of the error.

We finish these numerical studies by now considering the underlying method to be SIPG ($\kappa = -1$) everywhere except at the interface Γ_{HP}. In this case, there is a constraint on the size of the penalty parameter σ_F. First, we note that the

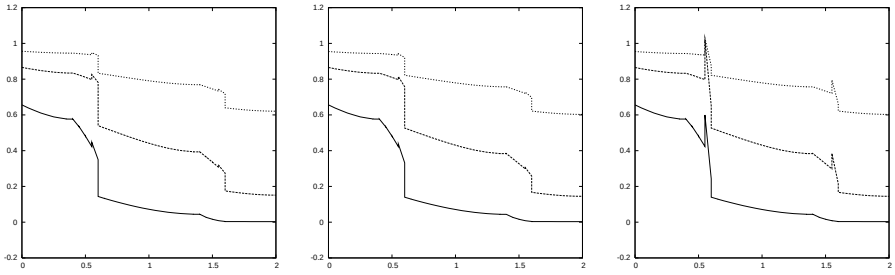

FIGURE 6. Explicit NIPG solution ($\kappa = 1, \sigma_F = 1$) with $d = d_\nu$: $\tilde{\kappa} = \tilde{\sigma}_\nu = 1$ (left), $\tilde{\kappa} = -1, \tilde{\sigma}_\nu = 1$ (center) and $\tilde{\kappa} = -1, \tilde{\sigma}_\nu = 10$ (right) at times t_0 (solid line), t_1 (dashed line) and t_2 (dotted line).

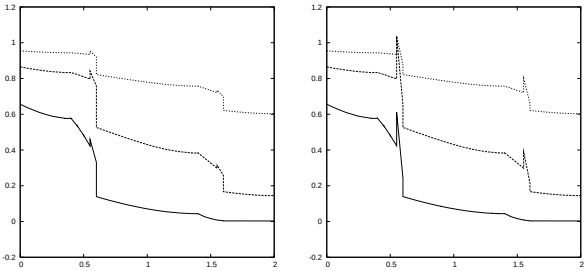

FIGURE 7. Explicit NIPG solution ($\kappa = 1, \sigma_F = 1$) with $d = d_\nu$ and $\tilde{\kappa} = 0$: $\tilde{\sigma}_\nu = 1$ (left) and $\tilde{\sigma}_\nu = 10$ (right) at times t_0 (solid line), t_1 (dashed line) and t_2 (dotted line).

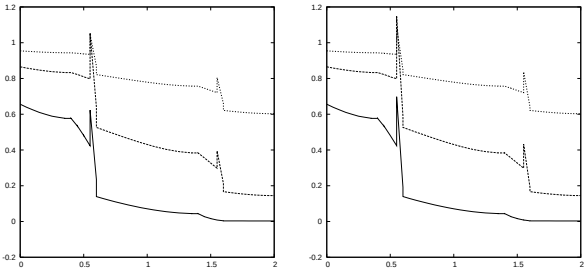

FIGURE 8. Explicit NIPG solution ($\kappa = 1, \sigma_F = 1$) with $d = d_\alpha$ and $\tilde{\kappa} = 0$: $\tilde{\sigma}_\alpha = 1$ (left) and $\tilde{\sigma}_\alpha = 10$ (right) at times t_0 (solid line), t_1 (dashed line) and t_2 (dotted line).

standard SIPG ($d = d_\alpha$ with $\tilde{\kappa} = -1$) on Γ_{HP} does not produce stable solutions even for large penalty values ($\sigma_F = \tilde{\sigma}_\alpha = 100$) if the explicit time discretization is used. However, the implicit time discretization stabilizes the method and the solutions are shown in Fig. 10 for linears and quadratics and for $\sigma_F = \tilde{\sigma}_\alpha = 10$. As in the case of the implicit NIPG method implemented on Γ_{HP}, (Fig. 4), the fronts are diffuse and instabilities occur when the polynomial degree is increased. If the optimal choice for the parameters in the definition of the adaptive flux is used, the resulting solution does not show any overshoot and the fronts remain sharp. The profiles for the implicit solution are shown in Fig. 11.

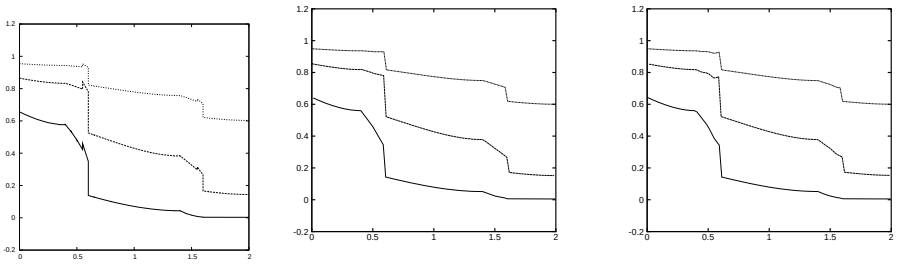

FIGURE 9. Adaptive NIPG solution with flux $d = d_\theta$: explicit $p = 1$ (left), implicit $p = 1$ (center) and implicit $p = 2$ (right), at times t_0 (solid line), t_1 (dashed line) and t_2 (dotted line).

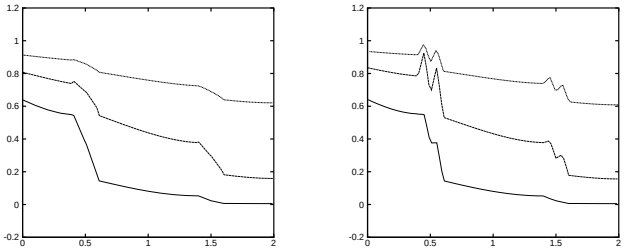

FIGURE 10. Implicit SIPG solution ($\kappa = \tilde{\kappa} = -1, \sigma_F = \tilde{\sigma} = 10$): $p = 1$ (left) and $p = 2$ (right), at times t_0 (solid line), t_1 (dashed line) and t_2 (dotted line).

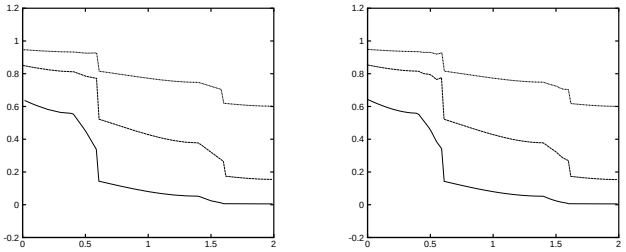

FIGURE 11. Implicit SIPG solution with ($\kappa = -1, \sigma_F = 10$) and adaptive flux $d = d_\theta$ ($\tilde{\kappa} = 1, \tilde{\sigma}_\nu = \epsilon_H, \tilde{\sigma}_\alpha = 1$): $p = 1$ (left) and $p = 2$ (right), at times t_0 (solid line), t_1 (dashed line) and t_2 (dotted line).

The conclusion of these numerical studies is that the improved and adaptive NIPG methods are more accurate than the standard NIPG method. One can also employ the SIPG method, but one has to carefully select the penalty parameter [11]. In what follows, we show that the adaptive method is the most accurate in the case of varying diffusivity.

6.2. Study of L^2 Errors. To complement our theoretical error analysis, we verify in this section the $l^\infty(L^2)$ accuracy of our improved and adaptive NIPG methods with respect to the exact solution.

By "exact", we mean an overkill solution where the mesh size is greatly refined and the number of finite elements is increased from 800 to 51,200. For stability of the numerical solution, the timestep must also be refined to 200 times smaller. We present results for an explicit time discretization and linear basis functions.

We consider two test problems. First, we compute the $l^\infty(L^2)$ error for the test problem described in the previous section. The errors for the standard, improved and adaptive NIPG methods are given in Table 1. Clearly the improved and adaptive solutions are more accurate than the standard NIPG solution. We also note that in this example, the improved solution yields the smallest error.

Method	Error
standard NIPG	1.0013×10^{-1}
improved NIPG	8.6381×10^{-3}
adaptive NIPG	1.3242×10^{-2}

TABLE 1. $l^\infty(L^2)$ errors for first test problem

The second test problem is a perturbation of the first test problem. We consider the same domain with the two vertical inclusions. However, we modify the value in the rightmost hyperbolic region from 10^{-3} to 0.5. This simple example demonstrates more realistic variations of diffusivity: in some places the diffusivity jump is large and in others small. Table 6.2 shows the errors in the $l^\infty(L^2)$ norm for the standard, improved and adaptive NIPG methods. Both improved and adaptive solutions have smaller errors than the standard NIPG solutions. However, in this case, the most accurate solution is the adaptive one. The adaptive NIPG method does a better job in capturing the exact solution on the interface where the diffusivity jump is nonzero but small, compared to the upwind NIPG method. Clearly the adaptive method is more advantageous in the case of highly varying diffusivity coefficient.

Method	Error
standard NIPG	1.0217×10^{-1}
improved NIPG	6.6179×10^{-2}
adaptive NIPG	1.1448×10^{-2}

TABLE 2. $l^\infty(L^2)$ errors for second test problem

6.3. Convergence Rates. In this section, we present numerical rates of convergence for a variety of diffusive fluxes, that confirm our theoretical error estimates.

The domain Ω is the unit square with a coarse mesh of 25 square elements ($h = 0.2$), containing a subdomain $\Omega_H = [0.4, 0.6] \times [0, 1]$ and $\Omega_P = \Omega \setminus \Omega_H$. The diffusion coefficients are constants where $\epsilon_P = 1$ and ϵ_H takes the value 10^{-8} or 10^{-4}. We consider the following smooth analytical solution:

$$\forall 0 \le x \le 0.4, \quad u(x) = \frac{\epsilon_H}{1.4 - 0.4\epsilon_H} x e^{x+t},$$

$$\forall 0.4 \le x \le 0.6, \quad u(x) = (x + 0.56\frac{\epsilon_H - 1}{1.4 - 0.4\epsilon_H}) e^{x+t},$$

$$\forall 0.6 \leq x \leq 1.0, \quad u(x) = ((1.6\epsilon_H - 0.6 + \frac{0.56(\epsilon_H - 1)^2}{1.4 - 0.4\epsilon_H})x + 0.6 + (0.56\frac{\epsilon_H - 1}{1.4 - 0.4\epsilon_H}) \\ -0.6(1.6\epsilon_H - 0.6 + \frac{0.56(\epsilon_H - 1)^2}{1.4 - 0.4\epsilon_H}))e^{x+t}.$$

The coarse mesh is successively uniformly refined, each triangle being divided into four triangles at each refinement stage. The time step is chosen small enough so that the numerical error is of the order of the spatial approximation error. We present rates obtained with the backward Euler discretization. The convergence rate is obtained as $log(e_h/e_{h/2})/log(2)$ where e_h is the numerical error obtained on the mesh with size h. We compute both H_1^0 and L^2-type errors defined below:

$$E_{h,1} = \frac{(\sum_{\Omega_e \in \mathcal{T}_h} \|\epsilon^{1/2}\nabla(u(T) - u_h(T))\|^2_{\Omega_e})^{1/2}}{(\sum_{\Omega_e \in \mathcal{T}_h} \|\epsilon^{1/2}\nabla u(T)\|^2_{\Omega_e})^{1/2}}, \quad E_{h,2} = \frac{\|u(T) - u_h(T)\|_\Omega}{\|u(T)\|_\Omega}$$

Table 3 contains the convergence rates for the case $\epsilon_H = 10^{-8}$ in the case of the NIPG method for several diffusive fluxes. Only the results for the finest mesh are given. For piecewise linear approximation, the finest mesh size is $h = 0.0125$ whereas for piecewise quadratic approximation, the finest mesh size is $h = 0.025$. In this experiment, the adaptive flux d_θ is defined with $\tilde{\kappa} = \tilde{\sigma}_\alpha = 1$ and $\tilde{\sigma}_\nu = \epsilon_H$. For the first five cases, the rates are optimal for the H_0^1 norm, as predicted by the theory. The cases $d = d_\alpha$ with $\tilde{\sigma}_\alpha = 1$ and $\tilde{\kappa} \in \{0, -1\}$ also yield optimal results for the energy norm. This means that the diffusion coefficient ϵ_H is small enough for these experiments. Finally, the last two cases should yield optimal results if the penalty is large enough. Clearly, this is the case for the choice $d = -\alpha + j_1$ but not the case for $d = d_\alpha$ with $\tilde{\kappa} = -1$ and $\tilde{\sigma}_\alpha = 1$ where we only obtain suboptimal energy rate for piecewise quadratic polynomials. For the L^2 norm, the rates are optimal for piecewise linear approximations and suboptimal for piecewise quadratics. Table 4 presents the convergence rates in the case of the SIPG method. In this case, the choice $\sigma_F = 1$ does not yield optimal rates and increasing the jump parameter to $\sigma_F = 10$, gives optimal rates both polynomial degrees and both norms. With the last two cases, the penalty parameter $\tilde{\sigma}$ was increased to 10 to obtain optimal rates.

6.4. Non-zero randomized diffusion. For this test problem, the diffusion coefficient is randomly selected to be either $\epsilon = 1$ or $\epsilon = 10^{-3}$ on each individual element using a random number generator (see Fig. 12). The velocity vector is $\beta = (1, 1)$, and consequently the inflow boundary consists of the left vertical boundary and bottom horizontal boundary. In all tests, a forward Euler in time and piecewise linear spatial discretization is used.

The adaptive technique, which automatically detects regions of numerical instability, is successful at producing an accurate and stable method without resorting to mesh refinement and consequently increased computational effort to maintain the integrity of the numerical solution. With this example, we demonstrate the complete failure of the standard NIPG method to achieve stability throughout the domain as well as the stability of both improved NIPG method and adaptive NIPG method.

In Fig. 16, we compare the standard NIPG solution with the improved NIPG solution extracted along the line $\{(x, 0.45) : 0 \leq x \leq 2\}$. As the progression of images clearly shows, the NIPG method tends to blow up after some finite time whereas the improved NIPG version is stable. Furthermore, in Fig. 17 we compare the profiles obtained with the improved method to the adaptive NIPG method The

Degree	$E_{h,1}$ rate	$E_{h,2}$ rate
	$d(u_h, v_h) = -\nu(u_h, v_h) + \nu(v_h, u_h) + j_1(u_h, v_h)$	
1	1.0015	2.0739
2	2.0011	2.3730
	$d(u_h, v_h) = -\nu(u_h, v_h) + \nu(v_h, u_h) + j_{\epsilon_H}(u_h, v_h)$	
1	1.0006	2.0274
2	1.9945	2.3567
	$d(u_h, v_h) = d_\theta(u_h, v_h)$ with $\tilde{\sigma}_\nu = \epsilon_H$	
1	1.0006	2.0274
2	1.9945	2.3567
	$d(u_h, v_h) = -\alpha(u_h, v_h) + \alpha(v_h, u_h) + j_1(u_h, v_h)$	
1	1.0026	2.0600
2	2.0004	2.4234
	$d(u_h, v_h) = -\nu(u_h, v_h) + j_1(u_h, v_h)$	
1	1.0015	2.0739
2	2.0011	2.3730
	$d(u_h, v_h) = -\nu(u_h, v_h) - \nu(v_h, u_h) + j_1(u_h, v_h)$	
1	1.0015	2.0739
2	2.0011	2.3730
	$d(u_h, v_h) = -\alpha(u_h, v_h) - \alpha(v_h, u_h) + j_1(u_h, v_h)$	
1	1.0019	2.0600
2	1.5751	2.4105
	$d(u_h, v_h) = -\alpha(u_h, v_h) + j_1(u_h, v_h)$	
1	1.0011	2.0598
2	2.0068	2.4446

TABLE 3. Case $\epsilon_H = 10^{-8}$: NIPG everywhere ($\kappa = 1, \sigma_F = 1$) except on interface Γ_{HP}.

lines are indistinguishable visually and demonstrate the stability of both methods. Two dimensional contours of the solution for all three methods (standard, improved and adaptive NIPG) are shown in Fig. 13, 14 and Fig. 15 respectively.

6.5. Vanishing randomized diffusion. Next, the diffusion coefficient is randomly selected to be either $\epsilon = 1$, $\epsilon = 10^{-3}$, or completely degenerate with $\epsilon = 0$ on each individual element using a random number generator (see Fig. 18). The velocity vector is $\beta = (1, 0)$, and consequently the inflow boundary consists of the left vertical boundary only. Fig. 19, 20 and 21 show the contours of the solutions obtained with the standard, improved and adaptive NIPG methods. Clearly the standard NIPG solution blows up after a few time steps whereas the improved and adaptive solutions remain stable throughout the simulation.

7. Conclusions

In this paper we analyze and develop discontinuous Galerkin methods for an advection-diffusion equation with spatially varying and possibly vanishing diffusion coefficient. Without resorting to slope limiting techniques nor mesh refinement, we demonstrate successful choices of numerical fluxes that appropriately capture solution behavior and minimize the L^2 norm of the error. We derived stability and a priori error estimates for both continuous and discrete time discretizations. Numerical tests indicate the robustness of our convergence estimates. Moreover,

Degree	$E_{h,1}$ rate	$E_{h,2}$ rate
	$d(u_h, v_h) = -\nu(u_h, v_h) + \nu(v_h, u_h) + j_1(u_h, v_h)$	
1	1.0016	2.0767
2	2.0084	2.9124
	$d(u_h, v_h) = -\nu(u_h, v_h) + \nu(v_h, u_h) + j_{\epsilon_H}(u_h, v_h)$	
1	1.0006	2.0291
2	2.0035	2.8742
	$d(u_h, v_h) = d_\theta(u_h, v_h)$ with $\tilde{\sigma}_\nu = \epsilon_H$	
1	1.0000	1.8989
2	2.0035	2.8742
	$d(u_h, v_h) = -\alpha(u_h, v_h) + \alpha(v_h, u_h) + j_1(u_h, v_h)$	
1	1.0010	1.9017
2	2.0209	2.9505
	$d(u_h, v_h) = -\nu(u_h, v_h) + j_{10}(u_h, v_h)$	
1	1.0014	2.0837
2	2.0081	2.9195
	$d(u_h, v_h) = -\nu(u_h, v_h) - \nu(v_h, u_h) + j_{10}(u_h, v_h)$	
1	1.0014	2.0837
2	2.0081	2.9195
	$d(u_h, v_h) = -\alpha(u_h, v_h) - \alpha(v_h, u_h) + j_{10}(u_h, v_h)$	
1	1.0012	2.0823
2	2.0075	2.9218
	$d(u_h, v_h) = -\alpha(u_h, v_h) + j_{10}(u_h, v_h)$	
1	1.0013	2.0817
2	2.0084	2.9235

TABLE 4. Case $\epsilon_H = 10^{-8}$: SIPG everywhere ($\kappa = -1, \sigma_F = 10$) except on interface Γ_{HP}.

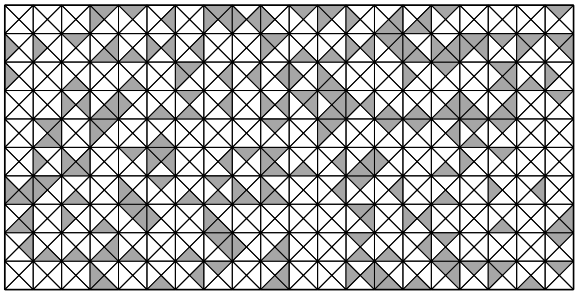

FIGURE 12. Mesh and diffusion coefficient randomly generated ($\epsilon_P = 1$ white, $\epsilon_H = 10^{-3}$ gray).

our numerical results indicate a substantial improvement in the solution for our adaptive flux technique over standard DG flux definitions.

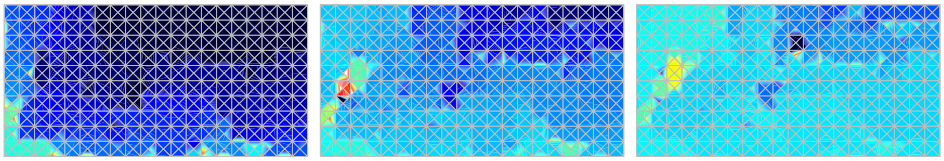

FIGURE 13. Two-dimensional contours with standard NIPG at times t_0 (left), t_1 (middle) and t_2 (right).

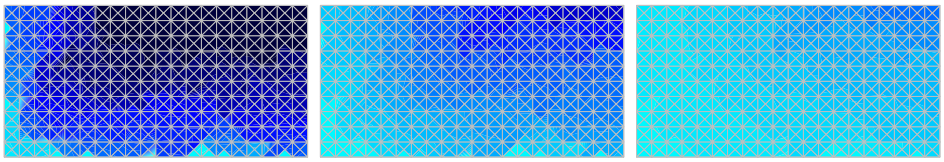

FIGURE 14. Two-dimensional contours with improved NIPG at times t_0 (left), t_1 (middle) and t_2 (right).

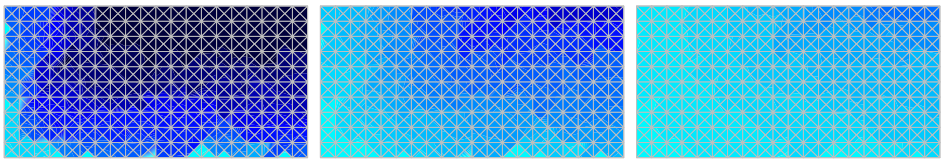

FIGURE 15. Two-dimensional contours with adaptive NIPG at times t_0 (left), t_1 (middle) and t_2 (right).

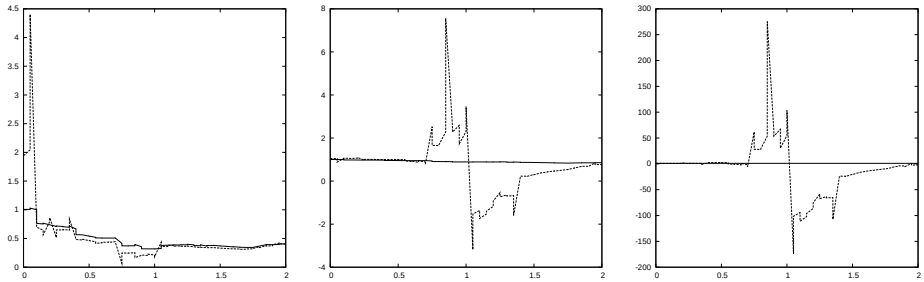

FIGURE 16. Comparison between standard NIPG (dashed line) and improved NIPG (solid line) at times t_0 (left), t_1 (middle) and t_2 (right).

References

[1] AIAA. Guide for verification and validation of computational fluid dynamics simulation. *Americal Institute of Aeronautics and Astronautics, Reston, VA*, Technical report AIAA G-077-1998, 1998.

[2] D.N. Arnold. An interior penalty finite element method with discontinuous elements. *SIAM J. Numer. Anal.*, 19:742–760, 1982.

[3] C.E. Baumann and J.T. Oden. A discontinuous hp finite element method for convection-diffusion problems. *Computer Methods Appl. Mech. Engrg.*, 175 (3-4):311–341, 1999.

[4] S.C. Brenner and L.R. Scott. *The Mathematical Theory of Finite Element Methods*, volume Texts in Applied Mathematics Vol. 15. Springer-Verlag, 1984.

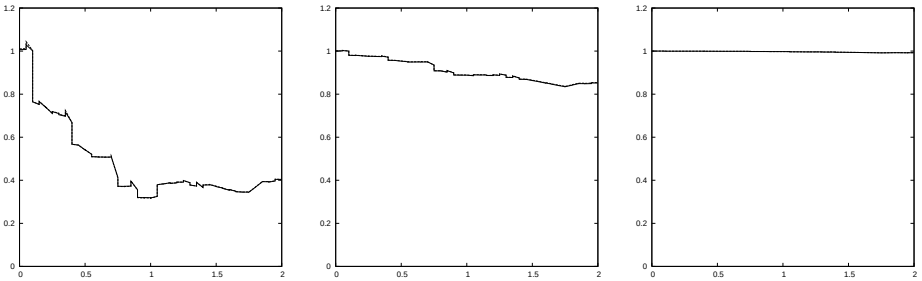

FIGURE 17. Comparison between improved NIPG (dashed line) and adaptive NIPG (solid line) solutions at at times t_0 (left), t_1 (middle) and t_2 (right).

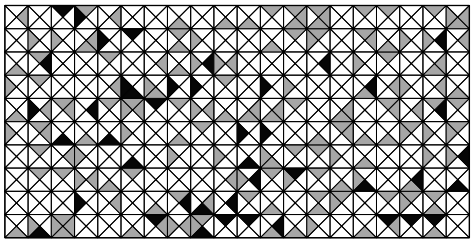

FIGURE 18. Mesh and diffusion coefficient randomly generated ($\epsilon_P = 1$ white, $\epsilon_H = 10^{-3}$ gray, $\epsilon_H = 0$ black).

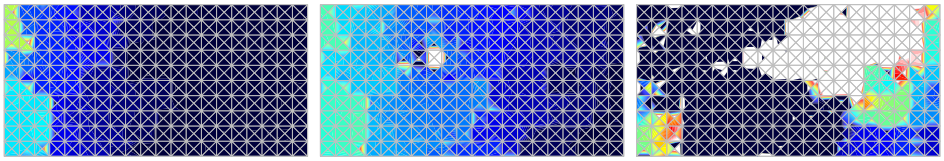

FIGURE 19. Two-dimensional contours with standard NIPG at times t_0 (left), t_1 (middle) and t_2 (right). White areas indicate values over 2.75.

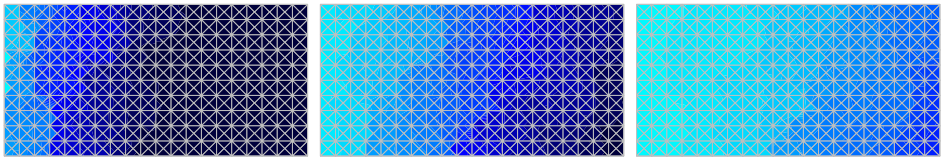

FIGURE 20. Two-dimensional contours with improved NIPG at times t_0 (left), t_1 (middle) and t_2 (right).

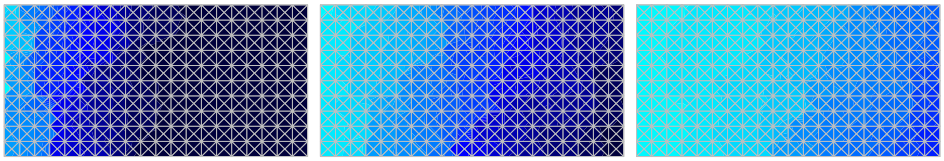

FIGURE 21. Two-dimensional contours with adaptive NIPG at times t_0 (left), t_1 (middle) and t_2 (right).

[5] B. Cockburn and C.N. Dawson. Some extensions of the local discontinuous Galerkin method for convection-diffusion equations in multidimensions. In J. Whiteman, editor, *Mathematics of Finite Elements and Applications: MAFELAP X*, pages 264–285. Elsevier, 2000.
[6] B. Cockburn and C.-W. Shu. The local discontinuous Galerkin method for time-dependent convection-diffusion systems. *SIAM J. Numer. Anal.*, 35:2440–2463, 1998.
[7] J.-P. Croisille, A. Ern, T. Lelièvre, and J. Proft. Analysis and simulation of a coupled hyperbolic/parabolic model problem. *Journal of Numerical Mathematics*, 13(2):81–103, 2005.
[8] C. Dawson, S. Sun, and M.F. Wheeler. Compatible algorithms for coupled flow and transport. *Comput. Meth. Appl. Mech. Eng.*, 193:2565–2580, 2004.
[9] A. Ern and J.-L. Guermond. *Theory and Practice of Finite Elements*, chapter Applied Mathematical Series Vol. 159. Springer-Verlag, 2004.
[10] A. Ern and J. Proft. Multi-algorithmic methods for coupled hyperbolic-parabolic problems. *International Journal of Numerical Analysis and Modeling*, 3(1):94–114, 2004.
[11] Y. Esphteyn and B. Rivière. Estimation of penalty parameters for symmetric interior penalty galerkin methods. submitted, also University of Pittsburgh technical report TR-MATH 06-05, 2006.
[12] A. Frati, F. Pasquarelli, and A. Quarteroni. Spectral approximation to advection-diffusion problems by the fictitious interface method. *J. comput. Phys.*, 107:201–212, 1993.
[13] F. Gastaldi and A. Quarteroni. On the coupling of hyperbolic and parabolic systems: Analytical and numerical approach. *Appl. Numer. Math.*, 6:3–31, 1989.
[14] P. Houston, C. Schwab, and E. Süli. Discontinuous hp-finite element methods for advection-diffusion problems. *SIAM J. Numer. Anal.*, 39(6):2133–2163, 2002.
[15] P. Houston, C. Schwab, and E. Suli. Stabilized hp-finite element methods for first-order hyperbolic problems. *SIAM J. Numer. Anal.*, 37:1618–1643, 2000.
[16] J. Douglas Jr. and T.F. Russell. Numerical methods for convection-diffusion problems based on combining the method of characteristics with finite element or finite difference procedures. *SIAM J. Numer. Anal.*, 19:871–885, 1982.
[17] D. Di Pietro, A. Ern, and J.-L. Guermond. Discontinuous galerkin methods for anisotropic semidefinite diffusion with advection. *SIAM J. Numer. Anal.*, 46:805–831, 2008.
[18] J. Proft and B. Rivière. Analytical and numerical study of diffusive fluxes for transport equations with near-degenerate coefficients. Technical Report TR-MATH 06-07, University of Pittsburgh, 2006.
[19] B. Rivière and M.F. Wheeler. Nonconforming methods for transport with nonlinear reaction. *Contemporary Mathematics*, 295:421–432, 2002.
[20] B. Rivière, M.F. Wheeler, and V. Girault. Improved energy estimates for interior penalty, constrained and discontinuous Galerkin methods for elliptic problems, part I. *Computational Geosciences*, 3:337–360, 1999.
[21] B. Rivière, M.F. Wheeler, and V. Girault. A priori error estimates for finite element methods based on discontinuous approximation spaces for elliptic problems. *SIAM J. Numer. Anal.*, 39(3):901–931, 2001.
[22] P.J. Roache. *Verification and validation in computational science and engineering*. Hermosa, Albuquerque, New Mexico, 1998.
[23] P. Siegel, R. Mosé, P. Ackerer, and J. Jaffre. Solution of the advection-diffusion equation using a combination of discontinuous and mixed finite elements. *Intl. J. Numer. Meth. Flu.*, 24:595–613, 1997.
[24] S. Sun and M.F. Wheeler. Symmetric and nonsymmetric discontinuous Galerkin methods for reactive transport in porous media. *SIAM J. Numerical Analysis*, 43(1):195–219, 2005.
[25] R.L. Trotta. Multidomain finite elements for advection-diffusion equations. *Appl. Numer. Math.*, 21:91–118, 1996.

ICES, The University of Texas at Austin, Austin, TX 78712
E-mail: jennifer@ices.utexas.edu

Department of Computational and Applied Mathematics, Rice University, Houston, TX 77005
E-mail: riviere@caam.rice.edu